Optimal Energy Management Strategies in Wireless Data and Energy Cooperative Communications

by

Jun Zhou
B.Eng., Beijing University of Posts and Telecommunications, 2015

A Thesis Submitted in Partial Fulfillment of the
Requirements for the Degree of

MASTER OF APPLIED SCIENCE

in the Department of Electrical and Computer Engineering

Optimal Energy Management Strategies in
Wireless Data and Energy Cooperative Communications

by

Jun Zhou
B.Eng., Beijing University of Posts and Telecommunications, 2015

Supervisory Committee

Dr. Xiaodai Dong, Supervisor
(Department of Electrical and Computer Engineering)

Dr. Wu-Sheng Lu, Co-Supervisor
(Department of Electrical and Computer Engineering)

Supervisory Committee

Dr. Xiaodai Dong, Supervisor
(Department of Electrical and Computer Engineering)

Dr. Wu-Sheng Lu, Co-Supervisor
(Department of Electrical and Computer Engineering)

ABSTRACT

This thesis first presents a new cooperative wireless communication network strategy that incorporates energy cooperation and data cooperation. The model establishment, design goal formulations, and algorithms for throughput maximization of the proposed protocol are presented and illustrated using a three-node network with two energy harvesting (EH) user nodes and a destination node. Transmission models are established from the performance analysis for a total of four scenarios. Based on the models, we seek to find optimal energy management strategies by jointly optimizing time allocation for each user, power allocations over these time intervals, and data throughputs at user nodes so as to maximize the sum-throughput or, alternatively, the minimum throughput of the two users in all scenarios. An accelerated Newton barrier algorithm and an alternative algorithm based on local quadratic approximation of the transmission models are developed to solve the aforementioned optimization problems. Then the thesis extends the cooperative strategy to multi-source wireless communication network, where N source users communicate with the destination via one relay that harvests energy from the RF signals transmitted by the sources through time-division multiple access (TDMA). We characterize the *Energy-Throughput* (E-T) tradeoff regions between the maximum achievable average throughput of the sources and the total amount of saved energy in three circumstances. For the case $N = 1$, all harvested energy will be used to forward the message. For the case $N > 1$, we compare two transmission strategies: one is common PS ratio strategy that the relay adopts the same PS ratio for all sources; the other is individual PS ratio strategy that each source uses an individual PS ratio. Numerical experiments under practical settings provide supportive evidences to our performance analysis.

Contents

List of Tables

List of Figures

List of Abbreviations

EH	Energy Harvesting
RF	Radio Frequency
SWIPT	Simultaneous Wireless Information and Power Transfer
ID	Information Decoding
TS	Time Switching
PS	Power Splitting
R-E	Rate-Energy
MIMO	Multiple-Input Multi-Output
WPCN	Wireless Powered Communication Networking
SNR	Signal-to-Noise Ratio
WD	Wireless Device
EC	Energy Cooperation
DC	Data Cooperation
DF	Decode-and-Forward
AF	Amplify-and-Forward
ET	Energy-Throughput
KKT	Karush-Kuhn-Tucker
NB	Newton Barrier

CP Convex Programming

QCQP Quadratically Constrained Quadratic Programming

QP Quadratic Programming

ACKNOWLEDGEMENTS

First of all, I would like to express my special thanks of gratitude to my supervisors Dr. *Xiaodai Dong* and Dr. *Wu-Sheng Lu*, who gave me the golden opportunity to study this wonderful research topic, energy harvesting. They have been supportive of my research goals and worked actively to provide me with insightful suggestions from both academic and industrial perspectives. They have taught me more than I could ever give them credit for here.

I am really thankful to Dr. Julie Zhou, my external departmental committee member, who has provided me extensive professional guidance and suggestions about scientific research and thesis writing in general.

I would like to thank my Manager *Derek Wang* and my mentor *Andre Furlan* in SAP, who provided me with great opportunities to learn industrial software development from wonderful data wrangling projects in analytics cloud. I have honed my programming skills and problem solving skills during that 8-month Co-op experience.

I am grateful to all of those colleagues with whom I have had the pleasure to work during my graduate studies: *Zheng Xu, Ming Lei, Leyuan Pan, Yongyu Dai, Binyan Zhao, Lan Xu, Le Liang, Weiheng Ni, Ping Cheng, Yiming Huo, Farnoosh Talaei, Tianyang Li, Yuejiao Hui, Wanbo Li, Wenyan Yu, Yizhou Zhu,* and *Minh Tu Hoang*; and friends with whom I have had good memories together during last two years in Victoria: *Guang Zeng, Zhu Ye, Xiao Xie, Yunlong Shao, Fang Chen, Xiao Ma, Mengyue Cai, Xiao Feng, Po Zhang* and *Feng Hu*.

With the deepest respect and love, I would thank my family, from whom I have derived the strength to challenge myself and perform better at each stage.

I have faced several challenges on my way during graduate studies, but each one of them has only strengthened me to make me the person I am today; someone who sets her eyes on a goal and does not lose sight of it, unless it is achieved. I will never slow down my steps to become the best person I can be.

Jun Zhou
Vancouver, BC
May, 2018

DEDICATION

To my mother
and
My grandparents
For your love and everything

Chapter 1

Introduction

1.1 Overview

1.1.1 Wireless Networks with Energy Harvesting

In traditional wireless communication networks such as wireless sensor networks, the wireless devices are powered by replaceable batteries with limited lifetime. To prolong the operating time of such wireless networks, energy harvesting (EH) technology has become an appealing solution in recent years. There are two main categories of energy sources to harvest, namely, (i) *ambient energy sources*, e.g., solar, wind energy and radio frequency (RF) energy, and (ii) *human power*, e.g., finger motion, breathing and blood pressure [5]. In outdoor environments, the most accessible energy sources are natural energy or environmental energy sources such as solar and wind energy [6]. However, harvesting natural energy presents a technical challenge because of the instability of the natural environment. By contrast, RF energy can provide sustainable and stable power supply, which is employed in increasingly emerging applications. Example applications of wireless communication networks with EH are illustrated in Fig. 1.1.

In an early research effort, natural energy is considered as the main EH energy source. Optimum transmission policies are studied in [7] to maximize the transmission throughput with limited battery storage constraint. In [8], optimal data transmission strategy is investigated for wireless EH nodes with finite battery capacity, which take into account quality of service (QoS) as well as the energy and data causality constraints altogether. Considering practical processing energy costs in [9], a "directional glue pouring algorithm" is developed to solve the proposed throughput maximization problems with multiple energy conditions and fading levels. In [10], optimal scheduling policies are developed under two

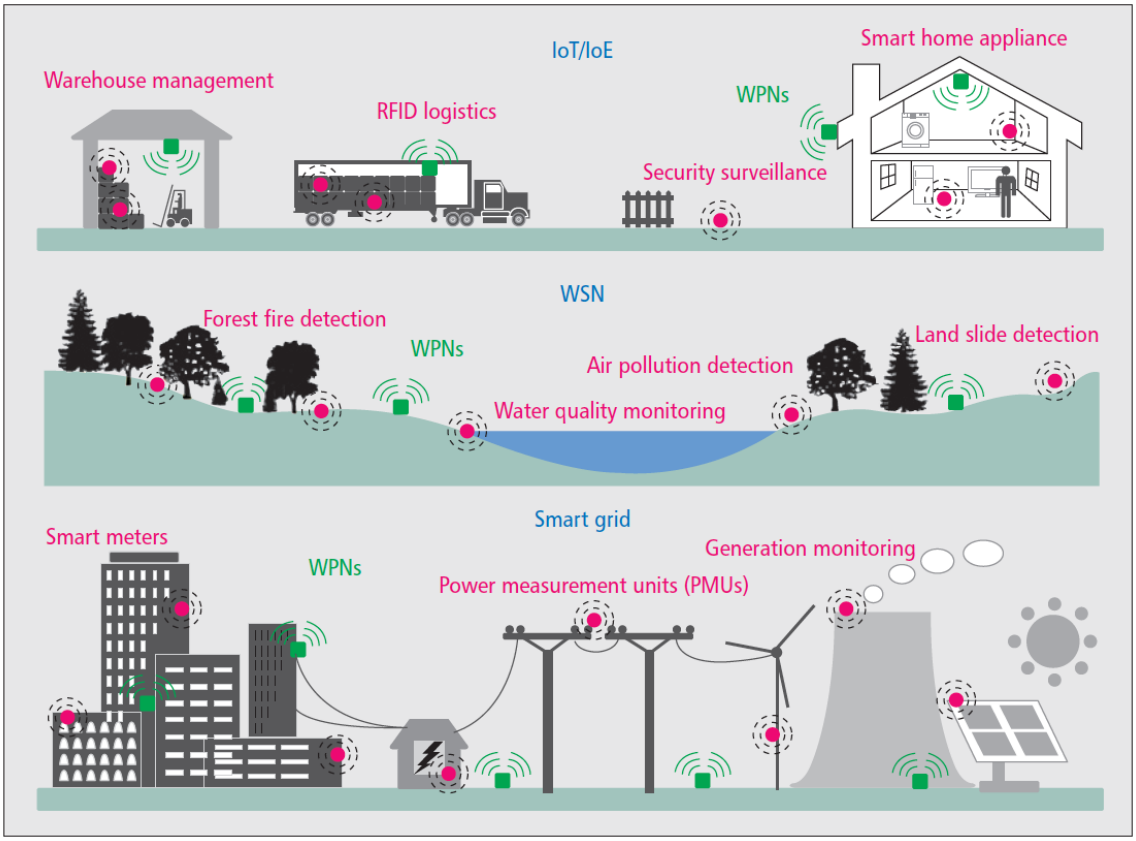

Figure 1.1: Example applications of wireless communication networks with EH: wireless power nodes in Internet of Things systems, wireless sensor networks for environment monitoring, and smart power grid. The green nodes denote wireless power nodes, which transmit RF energy to wireless powered devices, denoted by red nodes in the figure. [1]

data traffic scenarios, when all data bits have arrived before transmission or data bits arrive during transmissions. In terms of practical circuit model and transmission protocol, a *save-then-transmit* protocol is proposed in [11] where a save-ratio ρ of time T is used for energy harvesting by main energy storage device and the rest $(1-\rho)T$ time is used for data transmission.

The history of power transmission by radio waves is identified with emphasis upon the free-space microwave power transmission era beginning in 1958 [12]. It is only recently there has been an upsurge of research interests in RF energy harvesting/scavenging technique [13]. A general architecture of an RF energy harvesting network is shown in Fig. 1.2, where the solid arrow lines represent information flows, while the dashed arrow lines mean energy flows.

To address the energy shortage of solar powered wireless sensor networks during night-

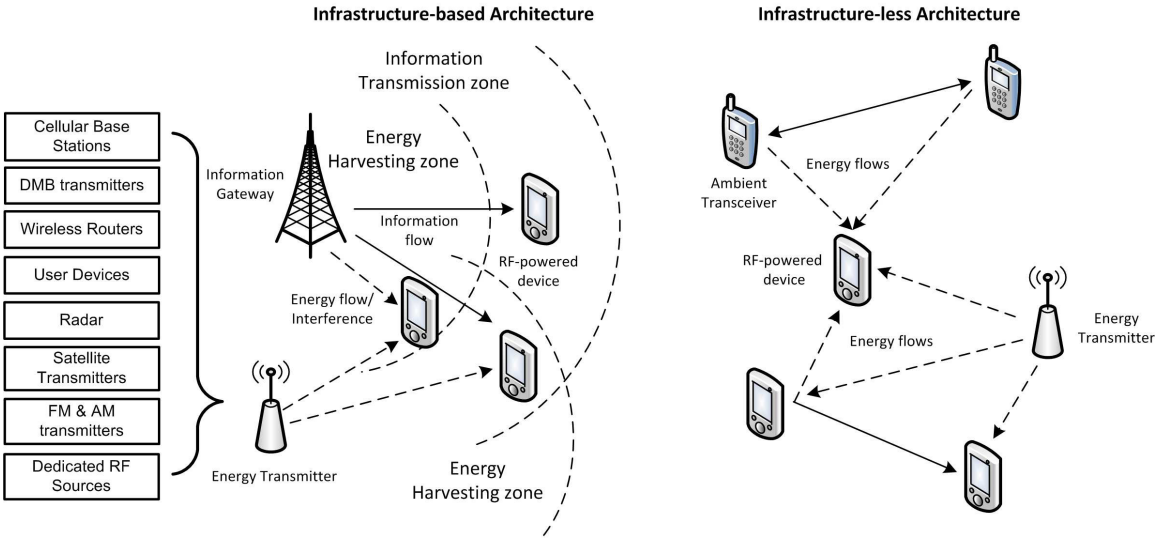

Figure 1.2: A general architecture of an RF energy harvesting network.

time, an effective RF energy harvesting wireless sensor network prototype is proposed in [14].

One important research direction in RF energy harvesting is simultaneous wireless information and power transfer (SWIPT) by RF signals. SWIPT realizes the efficient delivering of energy and information concurrently [13], and also brings tradeoffs between optimal energy transfer and information transmission. In practice, the received RF signal has to be split into two parts: one for EH, and the other for information decoding (ID). Two practical receiver schemes are proposed in [16] to separate energy and information parts: time switching (TS) and power splitting (PS) as shown in Fig. 1.3. To characterize the fundamental tradeoff between simultaneous data transmission and energy harvesting, a capacity-energy function is defined in [15]. Moreover, a rate-energy (R-E) region for a multiple-input multi-output (MIMO) wireless system is characterized in [16]. Based on TS scheme, optimal mode switching rules are derived based on the instantaneous channel gain and interference power in [17].

Another important research direction in RF energy harvesting is wireless powered communication networking (WPCN) where wireless devices are charged by RF signals from dedicated energy devices. Though WPCN has more reliable and sustainable power supply compared to the conventional battery-powered network, redesigns are still needed in many aspects. A brief overview of key challenges and solutions for WPCN designs are illustrated in [18], including doubly near-far problem, the signal-to-noise ratio (SNR) outage for the devices located toward the cell-edge, and etc. Schematics of key enhancing techniques for

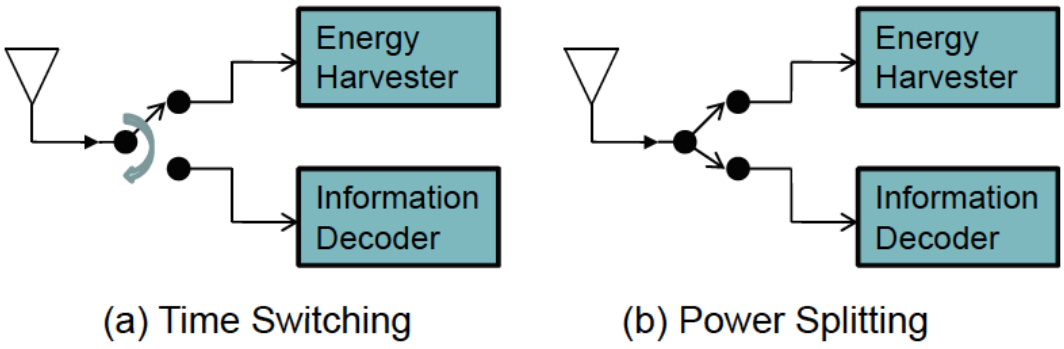

Figure 1.3: Four SWIPT transmission receiver schemes in different domains: a) time; b) power; c) antenna; d) space [16].

WPCN are proposed in [19]. The placement optimization of energy and information access points in WPCNs is investigated in [3] to reduce the network deployment cost and improve the performance effectively, where wireless devices (WDs) harvest the RF energy transferred by dedicated energy nodes in the downlink, and use the harvested energy to transmit data to information access points in the uplink shown in Fig. 1.4.

1.1.2 Cooperative Wireless Communications with Energy Harvesting

Challenged by dynamic environment and energy conditions, the problem of developing techniques to allocate the resources between different nodes efficiently has attracted lots of attention. Recently, efforts have been made to design cooperative and efficient energy management strategies in wireless networks with energy cooperation and relay cooperation.

Energy cooperation/sharing refers to techniques such that multiple devices can transfer energy to each other. In [20], *energy cooperation* (EC) is introduced that allows the EH source node to share some energy with the EH relay node. Furthermore, EC is extended to a two-way and multiple-access channel models in [21]. Two energy sharing mechanisms are discussed in [22]: direct energy transfer based schemes with wired energy sharing or wireless energy sharing, and non-direct energy transfer based schemes depending on traffic offloading and cooperative transmission techniques. In [23], energy sharing is also considered in a two-hop multi-access relay model, where transmitters are able to transfer energy to one another. In addition, the optimal solution to the energy transfer problem is shown to be an ordered node selection, where source nodes are prioritized over the strength

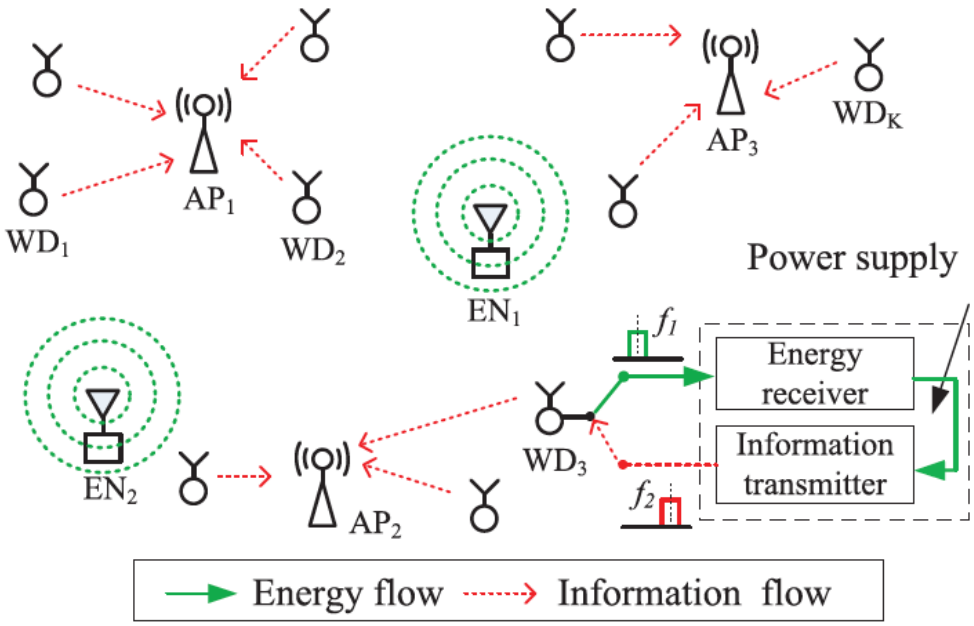

Figure 1.4: Schematics of a WPCN with separate ENs and APs. [3]

of their wireless and energy transfer channels. In [24], a cooperative multiple access model is considered where two EH transmitters can transfer energy to each other, while in [25], the EH transmitter and EH receiver can transfer a part of the stored energy to each other.

In terms of relay cooperation, multi-access and multi-hop communication networks are studied with one decode-and-forward (DF) EH relay and two parallel relays respectively in [4] as shown in Fig. 1.5. Furthermore, R-E region is derived at the multi-antenna EH relay in two-hop MIMO amplify-and-forward (AF) relay communication systems with SWIPT in [26]. Considering the spatial randomness of user locations in [27], outage probability experienced by users is characterized in a cooperative network with one EH relay, where the cooperation among users is modeled as a canonical coalitional game. In [28], two low-complexity dynamic antenna switching policies for SWIPT are proposed based on generalized selection combiner in MIMO relay channels, and the outage probability in closed-form expressions is derived. A wireless information and power transfer protocol is studied in a two-way AF relaying network in [29], where two source nodes exchange information through an RF-powered relay. Considering the network with a large number of randomly located transmitter-receiver pairs and potential DF relays, cooperative density and relay selection is investigated in a large-scale network with SWIPT in [30]. The outage

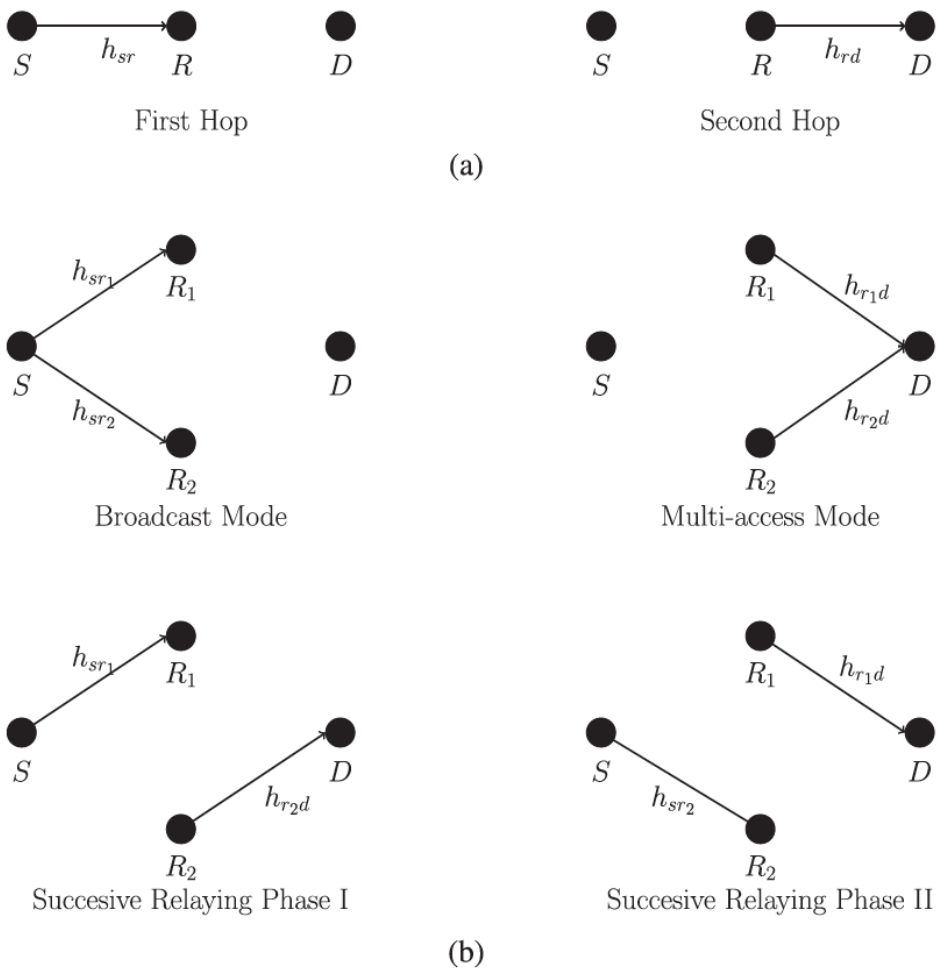

Figure 1.5: Transmission modes with (a) one relay, (b) two parallel relays [4].

performance and average harvested energy are derived in close-form in function of PS in both cooperative and non-cooperative schemes. In [31], optimum energy and information performance boundaries of a two-hop MIMO relay system are derived based on two scenarios. The first scenario assumes perfect CSI at receivers. The second scenario assumes only the second-order statistics of CSI at the transmitter.

1.2 Summary of Contributions

In this thesis, the main results are presented in Chapters 2 and 3, which are summarized below.

Chapter 2 presents a new cooperative wireless communication network strategy that incorporates energy cooperation and data cooperation. The model establishment, design goal formulations, and algorithms for throughput maximization of the proposed protocol are presented and illustrated using a three-node network with two EH user nodes and a destination node. Transmission models are established from the performance analysis for a total of four scenarios. Based on the models, we seek to find optimal energy management strategies by jointly optimizing time allocation for each user, power allocations over these time intervals, and data throughputs at user nodes so as to maximize the sum-throughput or, alternatively, the minimum throughput of the two users in all scenarios. An accelerated Newton barrier algorithm and an alternative algorithm based on local quadratic approximation of the transmission models are developed to solve the aforementioned optimization problems. Finally, numerical experiments under practical settings provide supportive observations to our performance analysis.

Chapter 3 investigates a new cooperative wireless communication network with multiple sources and one EH relay. Convex problems of characterizing the Energy-Throughput (E-T) tradeoffs between maximal amount of saved energy and achievable average throughput are formulated. When there is only one source node, the closed-form solution is derived by solving Karush-Kuhn-Tucker (KKT) conditions. When there are multiple source nodes, we propose two strategies: one is a common PS ratio strategy that the relay adopts the same PS ratio for all sources; the other is an individual PS ratio strategy that each source uses an individual optimal PS ratio for the performance.

1.3 Organizations

The rest of this thesis is organized as follows.

Chapter 2 considers a three node network with two EH user nodes and a destination node. The near user to the destination not only transmits its own message, but also forwards the far user's message to the destination. In addition, the far user also has direct communication with the destination. Two optimization algorithms to find optimal energy management strategies to maximize the sum-throughput and the minimum throughput of the two users are developed in Chapter 2.

Chapter 3 extends the three node network to a multiple-source network, where N source users communicate with the destination via one EH relay that harvests energy from the RF signals transmitted by the sources. The Energy-Throughput (E-T) tradeoff regions between the maximum achievable average throughput of the sources and the total amount of saved

energy are characterized based on two transmission strategies: one is common PS ratio strategy, and another is individual PS ratio strategy.

Chapter 4 concludes this thesis and enumerates open problems for further research.

Chapter 2

Optimal Energy Management Strategies in Wireless Communications with Joint Data and Energy Cooperation

2.1 Introduction

Energy harvesting (EH) has attracted significant interests from academia and industry in recent years, as both the concepts of green communication and practical needs from low power sensor networks are growing steadily. There are successful industrial EH products that harvest energy through light, kinetic motion, pressure, etc., for sensors and controls [32]. Harvesting natural energy, e.g., solar and wind energy [6], in general presents a reliability challenge because of the instability of the natural environment. There is much work in the literature on natural energy harvesting. In [33], two energy management strategies are proposed – one is to maximize the total throughput within a given time slot, and the other is to minimize the transmission completion time given target data throughputs. In [34], optimal online and offline energy management policies are designed by applying dynamic programming and staircase water-filling algorithm, respectively. Relative to natural resources of which EH can be greatly affected by environment changes, RF signals are more stable and human-controllable [13]. With rapid development and deployment of various wireless networks, contemporary radio wave energy harvesting techniques have emerged as promising solutions in the dealings with crucial energy constraint in battery-run networks. There are mainly two categories of RF wave based energy supply techniques. The first category is communication systems with simultaneous wireless information and

power transfer (SWIPT) first proposed in [16]. Because information and energy receivers are sensitive to different power values, two co-located receiver schemes for SWIPT, known as time switching (TS) and power splitting (PS), are described in [16]. Based on TS and PS receiver schemes, a general PS scheme termed dynamic PS (DPS) is proposed in [35, 36]. The second category is the RF-energy based wireless powered communication networking (WPCN) where wireless devices are charged by RF signals from a hybrid access point (H-AP) with power supply, first proposed in [37]. A "harvest-then-transmit" protocol is introduced in [37], where the sum-throughput maximization and common-throughput maximization are investigated. Recently, WPCN has emerged as an appealing candidate solution in future self-sustainable wireless communication systems [18, 19].

Furthermore, efforts have been made to design cooperative and efficient energy management strategies based on a three-node network including a relay, where both the EH source and EH relay harvest energy from nature in [20, 38–40]. In [20], an energy cooperation strategy is introduced that allows the EH source node to share some energy with the EH relay node. A wireless cooperative transmission scheme with *energy salvage* is proposed in [38], where the source can harvest energy from the relay signal transmitted to the destination. Under the decode-and-forward (DF) relaying scheme in [39], two optimal power allocation algorithms are developed to maximize the throughput with delay-constrained and no-delay-constrained traffic at the destination, respectively. Furthermore, short-term sum-rate maximization problems are solved in [40], where a two-way half-duplex relay channel is considered with DF relaying scheme.

Based on SWIPT techniques, the TS and PS protocols are also extended to three-node communication networks with relay assistance in [41–43]. Considering amplify-and-forwarding (AF) relaying in [41], the EH relay node has no other energy sources but uses TS or PS to split the received RF signal from the source into two streams, one for EH and the other for information forwarding. Considering both AF and DF schemes, the performance of EH and throughput are analyzed in [42], where the relay node uses TS to split received RF signals. Furthermore, under the DF relaying strategy, multiple source-destination pairs with only one relay are considered in [43], where the EH relay adopts PS to harvest energy from the RF signals transmitted from multiple sources. On the other hand, relay assistance is also applied to improve the performance of WPCN. In [44], "harvest-then-transmit" is extended to "harvest-then-cooperate" scheme that enables a relay node to forward the information transmission of the source node. Different from [44] where the relay node only transmits the information of the source, in [45] the "relay" node (the near user to H-AP) transmits its own data and forwards the information of the "far" user, which is called "user

cooperation".

Energy harvesting becomes even more relevant in a wireless sensor network for the rapidly increasing Internet of Things (IoT) applications. Many of these low power sensor nodes are distributed in areas with no power supply and expected to last for years running on battery and/or on EH from all available sources. Because nodes are located in different places, the energy they can harvest may differ as well. For example, a node that resides at a windy spot will harvest more wind energy than a neighboring node surrounded by structures. Therefore, not only data cooperation such as relaying will help to improve the overall performance of the network, RF energy cooperation/sharing will be an important approach to enhance the network operation. Another consideration is that the order in which the individual nodes transmit their messages with continuous EH supplies appear to impact the system's performance, because the nodes with more natural energy to harvest are supposed to transmit earlier and share its energy with those who need it. In this chapter, we are motivated to investigate the joint energy and data cooperation strategies in a multi-node sensor network, where each node harvests energy from natural environments as well as from each other. To enable tractable initial study, we consider a simple three node topology to illustrate the main idea, with potential extensions to more sophisticated network architectures in the future. The main contributions of this section are summarized below.

- A new cooperative wireless communication network strategy is proposed. The model establishment, design goal formulations, and algorithms for throughput maximization under the proposal are carried out and illustrated using a three-node network with two EH user nodes and a destination node. Transmission models are established based on performance analysis for a total of four scenarios, each with two cases to distinguish which of the two users transmits first, that take into account node activity status in terms of whether it transmits (we then call it active) while harvesting surrounding natural energy, or it does not transmit (then call it inactive) while harvesting natural energy as well as RF signals broadcast by the active user. In addition, the time-switching strategy adopted by the protocol allows a near-to-destination user to properly split the power of the RF signals from the "far" user, with one part for EH and the rest for relaying message to the destination. Collectively, this is a suite of transmission models for wireless networks with EH capabilities, where optimal throughputs can be achieved with the appropriate network cooperation strategy adaptive to the energy harvesting and propagation environments.

- Based on the proposed models, the problems of jointly optimizing the distribution

of time intervals for data cooperation and energy harvesting, power allocations over these time intervals, and data throughputs at user nodes so as to maximize the sum-throughput or, alternatively, the minimum throughput of the two users are formulated as convex constrained problems in all scenarios.

- Two fast algorithms are proposed to solve the aforementioned optimization problems. To be specific, an accelerated Newton barrier (NB) algorithm is developed to solve the constrained optimization problem, and the acceleration is achieved by a tailored line search technique which is required in each NB iteration. An alternative and often more efficient algorithm is developed based on a local approximation of the logarithmic terms involved. The results are convex quadratically constrained quadratic programming (QCQP) problems for several complex scenarios and quadratic programming (QP) problems for the rest of scenarios. Primal-dual path-following interior-point algorithms with closed-form line steps are deduced for these QCQP and QP problems and the efficiency of their implementations is evaluated and compared favorably with several available computer codes.

The rest of the chapter is organized as follows. Section 2.2 presents the system model that consists of channel model, EH model, and transmission models for four possible scenarios. Section 2.3 presents problem formulations based on the four scenarios, with the objective of maximizing the weighed sum-throughput and minimum throughput of the two users, respectively. In Section 2.4, we describe two convex optimization algorithms to solve the problems formulated in Section 2.3. Numerical results are given in Section 2.5 to evaluate how a wireless network in question performs with respect to the variations of the system parameters. Observations made from the simulation results are found supportive to our analysis. We conclude this chapter with a remark on notation: In what follows, $\log(\cdot)$ denotes the base-2 logarithm, and $\mathbb{E}[\cdot]$ denotes the statistical expectation.

2.2 System Model

As illustrated in Fig. 2.1, we consider a three-node network with two EH sensor nodes (called users) U_1, U_2 and a destination node D, each of which is equipped with a single antenna. Let d_i $(i = 1, 2)$ be the distance from U_i to D. Without loss of generality, we assume $d_1 < d_2$, and name U_1 and U_2 the *near user* and *far user*, respectively. Concerning the power supply status in the network, node D, simulating a gateway or data collector in a wireless sensor network, is powered by a stable energy supply, while the two sensor nodes

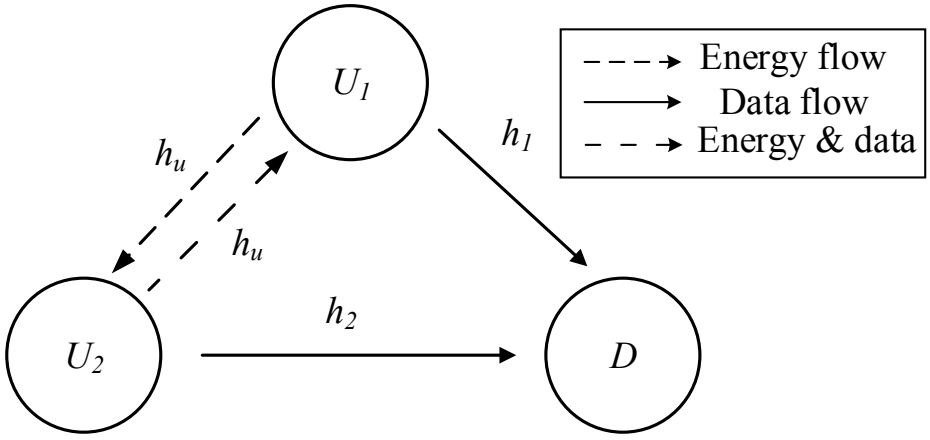

Figure 2.1: System model for a cooperative network with data cooperation and energy cooperation.

are powered by natural energy resources (e.g., solar, wind) as well as RF signals. The near user U_1 has data to send to the destination D, while the far user U_2 sends its data either directly to the destination or with the help of U_1 acting as a relay. The near user U_1 in our model acts as a decode-and-forward (DF) relay node and this message relaying process is called *data cooperation* (DC). Without data cooperation, U_2 must send with higher transmission power in order to reach D, compared with the relay mode. Data cooperation by U_1, however, will consume energy from U_1 and it is not directly obvious which method will result in higher sum throughput for U_1 and U_2 and lower total energy consumption. In this section, both users take advantage of RF energy harvesting whenever the other user is transmitting, which is referred to as *energy cooperation* (EC). Since information signal and energy signal are often in rather different power ranges, a time-switching (TS) technique is applied to separate information transmission and energy sharing. Specifically, the user will transmit information signal to the receiver with power P_i during ith time interval t_i and transmit energy signal to the other user with power P_{i+1} during t_{i+1}. This allows the system to effectively handle the scenario where P_{i+1} is considerably larger than P_i, which often occurs in practice.

2.2.1 Channel Model

Referring to the system model in Fig. 2.1, there are four channels in the network. Each channel can be characterized by a complex random variable $\tilde{h}$ with channel power gain $h = |\tilde{h}|^2$, which takes into account path loss and effects due to shadowing and channel fading. For simplicity, here we only consider the distance-dependent path loss so that the

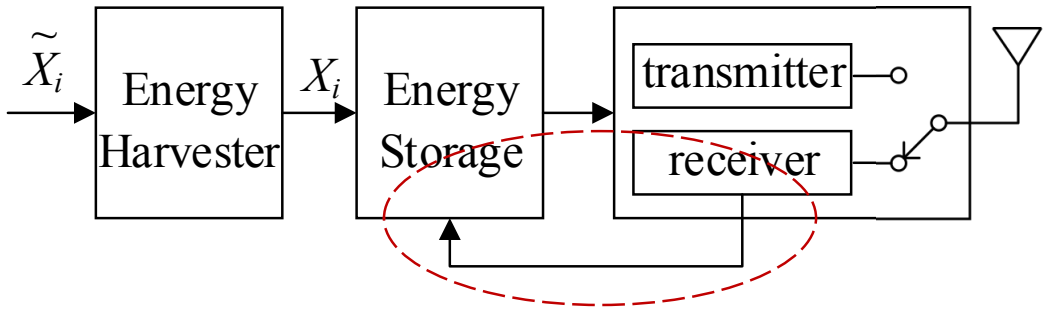

Figure 2.2: EH in a user node: $\tilde{X}_i$ is the rate of ambient natural energy arriving at user U_i and X_i the corresponding charging rate. The flow in the red circle indicates that the energy harvested from the received RF signals is also stored in the storage device before use, details of this are illustrated in Fig. 2.3.

channel power gain is modeled as $h = \lambda d^{-\alpha}$, where d is the distance from the transmitter to the receiver, α a path-loss exponent and λ an average signal power attenuation at a reference of 1 unit of distance.

We use $h_i = |\tilde{h}_i|^2$ $(i = 1, 2)$ to denote the power gain of the uplink channel from user U_i to D, and use $h_{ij} = |\tilde{h}_{ij}|^2$ $(i, j = 1, 2, i \neq j)$ for the power gain of the channel from U_i to U_j. Throughout we assume time-division multiple access (TDMA) is used for the data transmission among the nodes, hence the channel reciprocity holds, i.e., $h_{12} = h_{21}$, which we shall denote by h_u for simplicity.

Say the model is applicable to quasi-static block fading where the channel gains remain constant during each transmission block T, but may vary from one block to another. For convenience, $T = 1$ unit of time is assumed without loss of generality.

2.2.2 Energy Harvesting Model

Fig. 2.2 illustrates the energy harvesting and energy flow in a user node. The charging rate for user U_i is modeled as $X_i = \beta \tilde{X}_i$ with $0 \leq \beta \leq 1$ for $i = 1, 2$, where $\tilde{X}_i$ denotes the rate of natural energy arriving at user U_i and β is a constant specifying charging efficiency. In what follows, we assume that 1) the charging rates are equal to the associated arriving energy rates, i.e., $\beta = 1$; 2) the charging rates X_i remain constant during each transmission block T; 3) ideal storage devices are used to store the harvested energy without leakage so that the harvested energy is used fully for data transmission; and 4) both user nodes are able to transmit or receive signals and harvest ambient natural energy simultaneously.

Following the setup for TS techniques, two RF signal streams transmitted by the user nodes are used for information and energy transfer separately. As shown in Fig. 2.3,

the received information signal with power P_i is used for information decoding (ID), and another energy signal with P_{i+1} is used for EH in a subsequent interval. An example of a

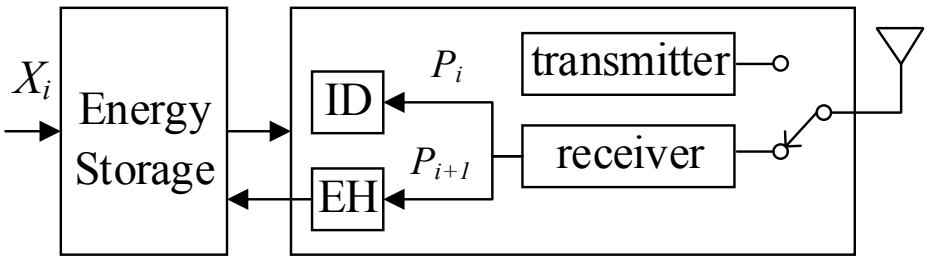

Figure 2.3: Receiver in a user node harvests and stores energy from RF signals.

possible scenario is that in a time duration t ($0 < t < T$) within a transmission block of length T, an inactive user harvests E_n from the natural energy and E_h from the RF energy signal with average transmission power P through a channel with power gain h. In such a case, we have

$$E_n = Xt \tag{2.1a}$$

$$E_h = \eta Pht \tag{2.1b}$$

where η is the energy harvesting efficiency [37].

2.2.3 Transmission Models

In order to be adaptive in different environmental circumstances, we propose to choose an optimal strategy from four scenarios: 1) Both DC and EC are applied; 2) Only DC is applied - the near user U_1 relays the information from U_2 to D, but no energy is harvested from RF signals; 3) Only EC is applied - all received RF signals from the other user are harvested but no data relay; 4) Neither DC nor EC occurs - each user is powered by natural energy and transmits information to D directly. Moreover, in each scenario we consider two cases: Case A when $X_1 \gg X_2$ and U_1 transmits first in order to share energy with U_2, and Case B when $X_2 \gg X_1$ hence U_2 transmits first in case to share energy with U_1. In the next section, by formulating and solving optimal power and time allocation for the eight combinations of energy-data cooperation and user node transmission order, the final optimal strategy will be obtained. In this section, the data transmission and energy harvesting protocol for each scenario and case are detailed. In the rest of the section, we use S1-A to represent case A of Scenario 1, etc.

Similar to the harvest-then-transmit protocol [37], for all four scenarios, we assume a possible initial time interval of length t_0 with $0 < t_0 < T$ when both users harvest natural energy before transmission.

Scenario 1: Both DC and EC are applied, see Fig. 2.1.

Case A: U_1 transmits first.

Each transmission block T consists of six non-overlapping time intervals of lengths $\{t_i, i = 0, 1, 2, 3, 4, 5\}$. In the rest of this section, we use superscript to denote which user node is transmitting and subscript to denote transmission time interval, e.g., $P_a^{(b)}$ to denote the average transmission power by sensor node U_b with $b = 1, 2$ during t_a with $a = 1, 2, 3, 4, 5$. The ID and EH activities at receivers in S1-A during time intervals t_1, t_2, t_3, t_4 and t_5 are summarized in Table 2.1. As a simple explanation of the table, during t_2, U_2 harvests the RF energy transmitted by U_1, hence in the $U_1 \rightarrow U_2$ column the box EH is marked with a ✓. Since U_2 is inactive, the boxes in the $U_2 \rightarrow D$ column and $U_2 \rightarrow U_1$ are in gray color with a backslash $\backslash$.

During t_1, U_1 transmits information signal to D with average power $P_1^{(1)}$, as well as harvests energy from natural resources. The complex baseband signal transmitted by U_1 is modeled as x_1 with $\mathbb{E}[|x_1|^2] = P_1^{(1)}$, which is received by D and U_2 as y_{10} and y_{12}, given by

$$y_{10} = \sqrt{h_1} x_1 + z_{10} \tag{2.2a}$$

$$y_{12} = \sqrt{h_u} x_1 + z_{12} \tag{2.2b}$$

where the noise terms are represented by $z_{10} \sim \mathcal{CN}(0, \sigma^2)$ and $z_{12} \sim \mathcal{CN}(0, \sigma_2^2)$, respectively. Due to *energy causality constraints* [33], U_1 cannot use the harvested energy during t_1 until t_2 starts, and hence the energy constraint

$$P_1^{(1)} t_1 \leq E_1 = X_1 t_0 \tag{2.3}$$

is imposed. On the other hand, U_2 remains inactive during t_1 and harvests natural energy. During the subsequent interval t_2, U_1 transmits energy signal to U_2 with average power $P_2^{(1)}$, hence the energy constraint during t_2 is given by

$$P_2^{(1)} t_2 \leq X_1 (t_0 + t_1) - P_1^{(1)} t_1. \tag{2.4}$$

During t_3, U_2 becomes active and broadcasts RF signals to U_1 and D with average power $P_3^{(2)}$. Let x_2 be the complex baseband signal transmitted by U_2 and $\mathbb{E}[|x_2|^2] = P_3^{(2)}$.

The corresponding received signals at D and U_1 can be expressed as

$$y_{20} = \sqrt{h_2}x_2 + z_{20} \tag{2.5a}$$

$$y_{21} = \sqrt{h_u}x_2 + z_{21} \tag{2.5b}$$

where $z_{20} \sim \mathcal{CN}(0, \sigma^2)$ and $z_{21} \sim \mathcal{CN}(0, \sigma_1^2)$ represents the noise at D and U_1. And the energy constraint at U_2 is given by

$$P_3^{(2)} t_3 \leq X_2(t_0 + t_1 + t_2) + \eta P_2^{(1)} h_u t_2. \tag{2.6}$$

During the next interval t_4, U_2 transmits energy signal to U_1 with average power $P_4^{(2)}$, and the energy constraint during t_4 is given by

$$P_4^{(2)} t_4 \leq X_2(t_0 + t_1 + t_2 + t_3) + \eta P_2^{(1)} h_u t_2 - P_3^{(2)} t_3. \tag{2.7}$$

During t_5, U_1 uses its remaining energy to relay U_2's message to D. The signal transmitted by U_1 is denoted as x_3 with $\mathbb{E}[|x_3|^2] = P_5^{(1)}$, which is received by D as y_{30}, namely

$$y_{30} = \sqrt{h_1}x_3 + z_{30}. \tag{2.8}$$

where $z_{30} \sim \mathcal{CN}(0, \sigma^2)$ represents the noise at D. The associated energy constraint during t_5 is given by

$$P_5^{(1)} t_5 \leq X_1(t_0 + t_1 + t_2 + t_3 + t_4) - P_1^{(1)} t_1 - P_2^{(1)} t_2 + \eta P_4^{(2)} h_u t_4. \tag{2.9}$$

Note that although U_2 harvests energy from natural energy during t_4, t_5 and U_1 is supposed to transfer energy to U_2 after t_5, the energy is stored for use in the next transmission block, and does not contribute to the current transmission block. It is for this reason this energy is not taken into account in the formulations of energy constraints.

Finally, in one block T, the amount of data transmission achievable by U_1 and U_2 can be expressed as

$$B_{1A} = t_1 \log(1 + \frac{P_1^{(1)} h_1}{\sigma^2}) = t_1 \log(1 + P_1^{(1)} \gamma_1) \tag{2.10a}$$

$$B_{2A} = \min[B_{2A}^{(2)} + B_{2A}^{(1)}, B_{2A}^{(u)}] \tag{2.10b}$$

respectively, where $\gamma_1 = \frac{h_1}{\sigma^2}$ [46]. And the amounts of data transmission achievable from

Table 2.1: ID and EH activities at receivers in S1-A.

	$U_1 \to D$	$U_1 \to U_2$	$U_2 \to D$	$U_2 \to U_1$	
	ID	EH	ID	ID	EH
t_1	U_1's message	\			
t_2	\	✓	\		
t_3	\		U_2's message		\
t_4	\				✓
t_5	U_2's message	\			

Table 2.2: ID and EH activities at receivers in S1-B.

	$U_1 \to D$	$U_1 \to U_2$	$U_2 \to D$	$U_2 \to U_1$	
	ID	EH	ID	ID	EH
t_1	\		U_2's message		\
t_2	\				✓
t_3	U_2's message	\			
t_4	U_1's message	\			

U_2 to D ($B_{2A}^{(2)}$), from U_1 to D ($B_{2A}^{(1)}$), and from U_2 to U_1 ($B_{2A}^{(u)}$) are given by

$$B_{2A}^{(2)} = t_3 \log(1 + \frac{P_3^{(2)} h_2}{\sigma^2}) = t_3 \log(1 + P_3^{(2)} \gamma_2) \tag{2.11a}$$

$$B_{2A}^{(1)} = t_5 \log(1 + \frac{P_5^{(1)} h_1}{\sigma^2}) = t_5 \log(1 + P_5^{(1)} \gamma_1) \tag{2.11b}$$

$$B_{2A}^{(u)} = t_3 \log(1 + \frac{P_3^{(2)} h_u}{\sigma_1^2}) = t_3 \log(1 + P_3^{(2)} \gamma_u) \tag{2.11c}$$

respectively, where $\gamma_2 = \frac{h_2}{\sigma^2}$ and $\gamma_u = \frac{h_u}{\sigma_1^2}$. It is worth noting that we focus on the case where the source-to-relay channel is better than the source-to-destination channel [46], so that $\gamma_u > \gamma_2$ is also imposed. Otherwise the relay U_1 should not play a role in the transmission from source U_2 to destination D.

Case B: U_2 transmits first.

In this case, each transmission block T consists of five non-overlapping time intervals, t_0, t_1, t_2, t_3 and t_4. Unlike Case A, however, during t_1, U_2 transmits RF signals with average power $P_1^{(2)}$. During t_2, U_2 transmits energy signal to U_1 with average power $P_2^{(2)}$.

Then during t_3, U_1 forwards U_2's message with average power $P_3^{(1)}$. And finally, U_1 transmits its own message with average power $P_4^{(1)}$ during t_4. Table 2.2 summarizes the ID and EH activities at receivers during t_1, t_2, t_3 and t_4.

At the end of the transmission block, the amount of data transmitted by U_1 and U_2,

denoted by B_{1B} and B_{2B} respectively, are given by

$$B_{1B} = t_4 \log(1 + P_4^{(1)}\gamma_1) \tag{2.12a}$$
$$B_{2B} = \min[B_{2B}^{(2)} + B_{2B}^{(1)}, B_{2B}^{(u)}] \tag{2.12b}$$
$$B_{2B}^{(2)} = t_1 \log(1 + P_1^{(2)}\gamma_2) \tag{2.12c}$$
$$B_{2B}^{(1)} = t_3 \log(1 + P_3^{(1)}\gamma_1) \tag{2.12d}$$
$$B_{2B}^{(u)} = t_1 \log(1 + P_1^{(2)}\gamma_u) \tag{2.12e}$$

where $B_{2B}^{(2)}, B_{2B}^{(1)}, B_{2B}^{(u)}$ denote the amounts of data transmission achievable from U_2 to D, from U_1 to D, and from U_2 to U_1, respectively. The energy constraints imposed on the active users are given by

$$P_1^{(2)} t_1 \leq X_2 t_0 \tag{2.13a}$$
$$P_2^{(2)} t_2 \leq X_2(t_0 + t_1) - P_1^{(2)} t_1 \tag{2.13b}$$
$$P_3^{(1)} t_3 \leq X_1(t_0 + t_1) + \eta P_2^{(2)} h_u t_2 \tag{2.13c}$$
$$P_4^{(1)} t_4 \leq X_1(t_0 + t_1 + t_2) + \eta P_2^{(2)} h_u t_2 - P_3^{(1)} t_3 \tag{2.13d}$$

Scenario 2: Only DC is applied, see Fig. 2.4.

In this scenario, the RF signals received at the relay node are utilized for ID without EC, and there are no time intervals allocated for energy sharing. Therefore, there are only four time intervals including t_0. The data throughputs and energy constraints for Cases A and B can readily be obtained by substituting $\eta = 0$ into (2.3), (2.6) and (2.9) - (2.13). The ID and EH activities during t_1, t_2 and t_3 are summarized in Table 2.3.

Table 2.3: ID activities at receivers in S2-A and S2-B with only DC.

		$U_1 \to D$	$U_2 \to D$	$U_2 \to U_1$
		ID	ID	ID
S2-A	t_1	U_1's message	\	
	t_2	\	U_2's message	
	t_3	U_2's message	\	
S2-B	t_1	\	U_2's message	
	t_2	U_2's message	\	
	t_3	U_1's message	\	

Scenario 3: Only EC is applied. See Fig. 2.5.

Each transmission block T in this scenario consists of four non-overlapping time inter-

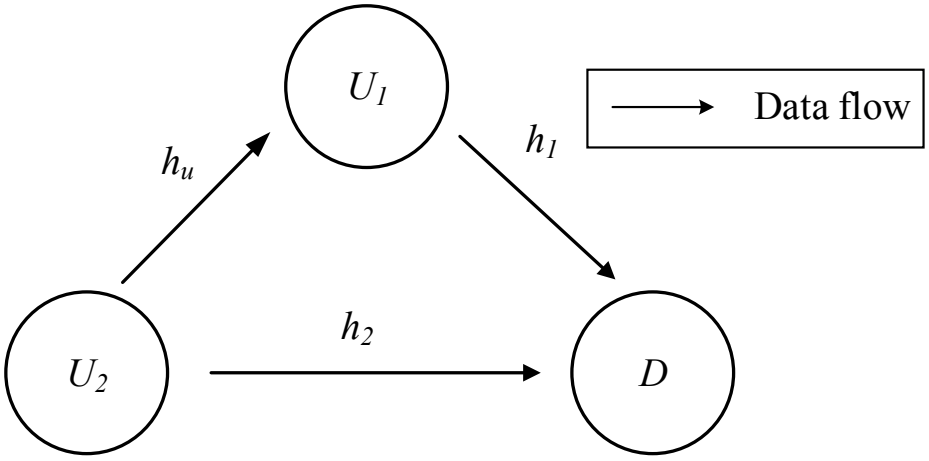

Figure 2.4: S2: Cooperative transmission model with data cooperation only.

vals t_0, t_1, t_2 and t_3. The two users broadcast their own message during t_1 and t_3, respectively. However, all RF signals received at the relay node are utilized for EH but with no data relay. The ID and EH activities at receivers are summarized in Table 3.11.

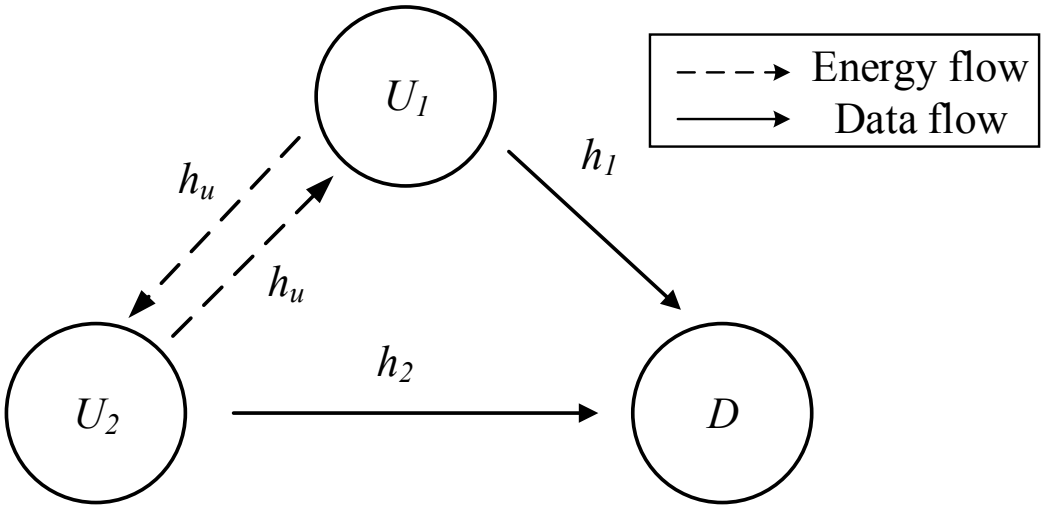

Figure 2.5: S3: Cooperative transmission model with energy cooperation only.

Under this circumstance, the achievable data transmission and associated energy constraints in Cases A and B can be expressed by

$$B_{1A} = t_1 \log(1 + P_1^{(1)}\gamma_1) \quad P_1^{(1)} t_1 \leq X_1 t_0 \tag{2.14a}$$

$$P_2^{(1)} t_2 \leq X_1(t_0 + t_1) - P_1^{(1)} t_1 \tag{2.14b}$$

$$B_{2A} = t_3 \log(1 + P_3^{(2)}\gamma_2) \quad P_3^{(2)} t_3 \leq X_2(t_0 + t_1 + t_2) + \eta P_2^{(1)} h_u t_2 \tag{2.14c}$$

Table 2.4: ID and EH activities at receivers in S3-A and S3-B with only EC.

		$U_1 \to D$	$U_1 \to U_2$	$U_2 \to D$	$U_2 \to U_1$
		ID	EH	ID	EH
S3-A	t_1	U_1's message		\	
	t_2	\	✓	\	
	t_3	\		U_2's message	\
S3-B	t_1	\		U_2's message	\
	t_2	\		\	✓
	t_3	U_1's message		\	

$$B_{2B} = t_1 \log(1 + P_1^{(2)}\gamma_2) \quad P_1^{(2)} t_1 \leq X_2 t_0 \tag{2.14d}$$

$$P_2^{(2)} t_2 \leq X_2(t_0 + t_1) - P_1^{(2)} t_1 \tag{2.14e}$$

$$B_{1B} = t_3 \log(1 + P_3^{(1)}\gamma_1) \quad P_3^{(1)} t_3 \leq X_1(t_0 + t_1 + t_2) + \eta P_2^{(2)} h_u t_2 \tag{2.14f}$$

Scenario 4: Neither DC nor EC occurs.

Here, U_1 and U_2 transmit their own messages to D directly during t_1 and t_2. The data throughputs and energy constraints in S4-A and B can readily be established by substituting $\eta = 0$ into (2.14).

2.3 Convex Problem Formulation

Given natural energy arrival rates at the two user nodes and channel conditions, we seek to determine an optimal scenario in which the distribution of time intervals $\{t_i\}$, power allocations over these time intervals, and data throughputs at the user nodes are jointly optimized so as to maximize the weighted sum-throughput over the present transmission block subject to the constraints imposed for the chosen scenario. We focus on weighted sum-throughput because it helps to give more attention to the sensor node with higher priority in a practical network. An alternative goal instead of weighted sum-throughput maximization is to maximize the minimum throughput of the two users [37]. In this section we present two sets of problem formulations. Based on the analysis and models established in Section 2.2, the joint optimization problem is formulated for each EC-DC scenario. As will be shown below, these optimization problems turn out to be convex after a simple variable substitution, hence admit reliable algorithms. The optimal scenario can therefore be identified by evaluating the solutions obtained. Furthermore, based on a second-order approximation of the two-variable *"logarithmic perspective"*, we derive a set of approximate problem formulations. The simplified quadratic formulations remain convex. Both problem formulations,

original and approximate, have fast solutions which are developed in Section 2.4.

2.3.1 Convex formulations based on the models from Section II

(1) Weighted sum-throughput maximization

The objective here is to maximize the weighted sum throughput over one transmission block with given throughput weights $\boldsymbol{w} = [w_1, w_2]$, by jointly optimizing power and time allocations for each of the four transmission scenarios. The sensor node U_i with larger weight w_i has higher priority.

In Scenario S1, the design variables are time allocation $\boldsymbol{t} = [t_0, t_1, t_2, t_3, t_4, t_5]$, power allocations $\boldsymbol{P}_A = [P_1^{(1)}, P_2^{(1)}, P_3^{(2)}, P_4^{(2)}, P_5^{(1)}]$, $\boldsymbol{P}_B = [P_1^{(2)}, P_2^{(2)}, P_3^{(1)}, P_4^{(1)}]$, and throughputs $\boldsymbol{B}_A = [B_{1A}, B_{2A}, B_{2A}^{(1)}, B_{2A}^{(2)}, B_{2A}^{(u)}]$, $\boldsymbol{B}_B = [B_{1B}, B_{2B}, B_{2B}^{(1)}, B_{2B}^{(2)}, B_{2B}^{(u)}]$. Based on the model for S1 in Section 2.2, the problems at hand for S1-A and B can be formulated, respectively, as

$$\underset{\boldsymbol{t},\boldsymbol{P}_A,\boldsymbol{B}_A}{\text{maximize}} \quad w_1 B_{1A} + w_2 B_{2A} \tag{2.15a}$$

$$\text{s.t.} \quad B_{2A} \le B_{2A}^{(2)} + B_{2A}^{(1)} \tag{2.15b}$$

$$B_{2A} \le B_{2A}^{(u)} \tag{2.15c}$$

$$(2.3), (2.4), (2.6), (2.7), (2.9), (2.10), (2.11) \tag{2.15d}$$

$$t_0 + t_1 + t_2 + t_3 + t_4 + t_5 = 1 \tag{2.15e}$$

$$t_i \ge 0, i = 0, 1, 2, 3, 4, 5 \tag{2.15f}$$

and

$$\underset{\boldsymbol{t},\boldsymbol{P}_B,\boldsymbol{B}_B}{\text{maximize}} \quad w_1 B_{1B} + w_2 B_{2B} \tag{2.16a}$$

$$\text{s.t.} \quad B_{2B} \le B_{2B}^{(2)} + B_{2B}^{(1)} \tag{2.16b}$$

$$B_{2B} \le B_{2B}^{(u)} \tag{2.16c}$$

$$(2.12), (2.13) \tag{2.16d}$$

$$t_0 + t_1 + t_2 + t_3 + t_4 = 1 \tag{2.16e}$$

$$t_i \ge 0, i = 0, 1, 2, 3, 4 \tag{2.16f}$$

We note that the objective functions in (2.15) and (2.16) are in the form $t \log(1 + \gamma P)$ which is not concave with respect to t and P. However, by using variable substitution $y = Pt$ [45] and considering $\{t, y\}$ as the design variables instead of $\{t, P\}$, the objective

assumes the form $t\log(1+\gamma\frac{y}{t})$ which is the *perspective* of concave function $f(x)=\log(1+\gamma x)$. It then follows from Section 3.2.6 of [47] that $g(y,t)=t\log(1+\gamma\frac{y}{t}), t>0$ is also concave with respect to variables t and y. The same argument applies to the constraints in problems (2.15) and (2.16) that the variable change $y=Pt$ assures that all constraints involved are convex.

Also note that the constraints in (2.15e) can be used to eliminate t_0 from these problems by substituting t_0 by $1-(t_1+t_2+t_3+t_4+t_5)$ and imposing the non-negativity constraint $1-(t_1+t_2+t_3+t_4+t_5)\geq 0$. In doing so, the problems in (2.15) and (2.16) are simplified convex problems as follows, where (P1-A) and (P1-B) denote "Problem for Scenario 1, Case A" and "Problem for Scenario 1, Case B", respectively:

$$\text{(P1-A)}\quad \underset{\boldsymbol{t},\boldsymbol{y},\boldsymbol{B}_{2A}}{\text{maximize}} \quad w_1 t_1\log(1+\gamma_1\frac{y_1}{t_1})+w_2 B_{2A} \tag{2.17a}$$

$$\text{s.t.} \quad B_{2A}\leq t_3\log(1+\gamma_2\frac{y_3}{t_3})+t_5\log(1+\gamma_1\frac{y_5}{t_5}) \tag{2.17b}$$

$$B_{2A}\leq t_3\log(1+\gamma_u\frac{y_3}{t_3}) \tag{2.17c}$$

$$y_1\leq X_1(1-t_1-t_2-t_3-t_4-t_5) \tag{2.17d}$$

$$y_2\leq X_1(1-t_2-t_3-t_4-t_5)-y_1 \tag{2.17e}$$

$$y_3\leq X_2(1-t_3-t_4-t_5)+\eta h_u y_2 \tag{2.17f}$$

$$y_4\leq X_2(1-t_4-t_5)+\eta h_u y_2-y_3 \tag{2.17g}$$

$$y_5\leq X_1(1-t_5)-y_1-y_2+\eta h_u y_4 \tag{2.17h}$$

$$t_1+t_2+t_3+t_4+t_5\leq 1 \tag{2.17i}$$

$$t_i\geq 0, y_i\geq 0, i=1,2,3,4,5 \tag{2.17j}$$

$$\text{(P1-B)}\quad \underset{\boldsymbol{t},\boldsymbol{y},\boldsymbol{B}_{2B}}{\text{maximize}} \quad w_1 t_4\log(1+\gamma_1\frac{y_4}{t_4})+w_2 B_{2B} \tag{2.18a}$$

$$\text{s.t.} \quad B_{2B}\leq t_1\log(1+\gamma_2\frac{y_1}{t_1})+t_3\log(1+\gamma_1\frac{y_3}{t_3}) \tag{2.18b}$$

$$B_{2B}\leq t_1\log(1+\gamma_u\frac{y_1}{t_1}) \tag{2.18c}$$

$$y_1\leq X_2(1-t_1-t_2-t_3-t_4) \tag{2.18d}$$

$$y_2\leq X_2(1-t_2-t_3-t_4)-y_1 \tag{2.18e}$$

$$y_3\leq X_1(1-t_3-t_4)+\eta h_u y_2 \tag{2.18f}$$

$$y_4\leq X_1(1-t_4)+\eta h_u y_2-y_3 \tag{2.18g}$$

$$t_1 + t_2 + t_3 + t_4 \leq 1 \tag{2.18h}$$

$$t_i \geq 0, y_i \geq 0, i = 1, 2, 3, 4 \tag{2.18i}$$

For S2, the formulations of the weighted throughput maximization problems are obtained by

$$\text{(P2-A)} \quad \underset{\boldsymbol{t},\boldsymbol{y},\boldsymbol{B}_{2A}}{\text{maximize}} \quad w_1 t_1 \log(1 + \gamma_1 \frac{y_1}{t_1}) + w_2 B_{2A} \tag{2.19a}$$

$$\text{s.t.} \quad B_{2A} \leq t_2 \log(1 + \gamma_2 \frac{y_2}{t_2}) + t_3 \log(1 + \gamma_1 \frac{y_3}{t_3}) \tag{2.19b}$$

$$B_{2A} \leq t_2 \log(1 + \gamma_u \frac{y_2}{t_2}) \tag{2.19c}$$

$$y_1 \leq X_1(1 - t_1 - t_2 - t_3) \tag{2.19d}$$

$$y_2 \leq X_2(1 - t_2 - t_3) \tag{2.19e}$$

$$y_3 \leq X_1(1 - t_3) - y_1 \tag{2.19f}$$

$$t_1 + t_2 + t_3 \leq 1 \tag{2.19g}$$

$$t_i \geq 0, y_i \geq 0, i = 1, 2, 3 \tag{2.19h}$$

and

$$\text{(P2-B)} \quad \underset{\boldsymbol{t},\boldsymbol{y},\boldsymbol{B}_{2B}}{\text{maximize}} \quad w_1 t_3 \log(1 + \gamma_1 \frac{y_3}{t_3}) + w_2 B_{2B} \tag{2.20a}$$

$$\text{s.t.} \quad B_{2B} \leq t_1 \log(1 + \gamma_2 \frac{y_1}{t_1}) + t_2 \log(1 + \gamma_1 \frac{y_2}{t_2}) \tag{2.20b}$$

$$B_{2B} \leq t_1 \log(1 + \gamma_u \frac{y_1}{t_1}) \tag{2.20c}$$

$$y_1 \leq X_2(1 - t_1 - t_2 - t_3) \tag{2.20d}$$

$$y_2 \leq X_2(1 - t_2 - t_3) - y_1 \tag{2.20e}$$

$$y_3 \leq X_1(1 - t_3) \tag{2.20f}$$

$$t_1 + t_2 + t_3 \leq 1 \tag{2.20g}$$

$$t_i \geq 0, y_i \geq 0, i = 1, 2, 3 \tag{2.20h}$$

For S3-A, it follows from the model in Section 2.2 (see (2.14)) and Table 3.11 that the throughput maximization problem assumes the form

$$\text{(P3-A)} \quad \underset{\boldsymbol{t},\boldsymbol{y}}{\text{maximize}} \quad w_1 t_1 \log(1 + \gamma_1 \frac{y_1}{t_1}) + w_2 t_3 \log(1 + \gamma_2 \frac{y_3}{t_3}) \tag{2.21a}$$

$$\text{s.t.} \quad y_1 \leq X_1(1 - t_1 - t_2 - t_3) \tag{2.21b}$$

$$y_2 \le X_1(1-t_2-t_3) - y_1 \tag{2.21c}$$
$$y_3 \le X_2(1-t_3) + \eta h_u y_2 \tag{2.21d}$$
$$t_1 + t_2 + t_3 \le 1 \tag{2.21e}$$
$$t_i \ge 0, y_i \ge 0, i = 1,2,3 \tag{2.21f}$$

Similarly, the optimization problem for S3-B can be formulated as

$$\text{(P3-B)} \quad \underset{\boldsymbol{t},\boldsymbol{y}}{\text{maximize}} \quad w_1 t_3 \log(1+\gamma_1 \frac{y_3}{t_3}) + w_2 t_1 \log(1+\gamma_2 \frac{y_1}{t_1}) \tag{2.22a}$$
$$\text{s.t.} \quad y_1 \le X_2(1-t_1-t_2-t_3) \tag{2.22b}$$
$$y_2 \le X_2(1-t_2-t_3) - y_1 \tag{2.22c}$$
$$y_3 \le X_1(1-t_3) + \eta h_u y_2 \tag{2.22d}$$
$$t_1 + t_2 + t_3 \le 1 \tag{2.22e}$$
$$t_i \ge 0, y_i \ge 0, i = 1,2,3 \tag{2.22f}$$

The problem formulations for S4, where no cooperation occurs, can be simply formulated as

$$\text{(P4-A)} \quad \underset{\boldsymbol{t},\boldsymbol{y}}{\text{maximize}} \quad w_1 t_1 \log(1+\gamma_1 \frac{y_1}{t_1}) + w_2 t_2 \log(1+\gamma_2 \frac{y_2}{t_2}) \tag{2.23a}$$
$$\text{s.t.} \quad y_1 \le X_1(1-t_1-t_2) \tag{2.23b}$$
$$y_2 \le X_2(1-t_2) \tag{2.23c}$$
$$t_1 + t_2 \le 1 \tag{2.23d}$$
$$t_i \ge 0, y_i \ge 0, i = 1,2 \tag{2.23e}$$

$$\text{(P4-B)} \quad \underset{\boldsymbol{t},\boldsymbol{y}}{\text{maximize}} \quad w_1 t_2 \log(1+\gamma_1 \frac{y_2}{t_2}) + w_2 t_1 \log(1+\gamma_2 \frac{y_1}{t_1}) \tag{2.23f}$$
$$\text{s.t.} \quad y_1 \le X_2(1-t_1-t_2) \tag{2.23g}$$
$$y_2 \le X_1(1-t_2) \tag{2.23h}$$
$$t_1 + t_2 \le 1 \tag{2.23i}$$
$$t_i \ge 0, y_i \ge 0, i = 1,2 \tag{2.23j}$$

(2) Maximization of least throughput of the two users

As an alternative goal to the sum-throughput maximization addressed above, we may

consider the problem of maximizing the least throughput of the two users. Problem of this type is known as the common-throughput maximization [37], and is regarded as useful as it facilitates balancing the resources between the two users. Denote the individual throughputs of users U_1 and U_2 by B_1 and B_2, respectively, and let $\boldsymbol{B} = [B_1, B_2]$, the common-throughput maximization problem can be formulated as

$$\text{(P5)} \quad \underset{\boldsymbol{t},\boldsymbol{y},\boldsymbol{B},\bar{B}}{\text{maximize}} \quad \bar{B} \tag{2.24a}$$

$$\text{s.t.} \quad \bar{B} \leq B_i, i = 1, 2 \tag{2.24b}$$

$$\boldsymbol{B} \in \Phi, \boldsymbol{t} \in \Psi, \boldsymbol{y} \in \Omega \tag{2.24c}$$

where Φ, Ψ and Ω are the feasible sets for throughputs $\boldsymbol{B}$, time allocation $\boldsymbol{t}$ and auxiliary variable $\boldsymbol{y}$, respectively, that can be further specified in accordance with a given scenario. Regardless of the specific scenario involved, B_i's in (2.24b) always assume the form $t\log(1+\gamma\frac{y}{t})$, hence the constraints in (2.24b) are convex.

2.3.2 Convex quadratic formulations

(1) Quadratic approximation of the perspective function

The logarithmic perspective function

$$l_\gamma(t, y) = -t\log(1 + \frac{\gamma y}{t}) \tag{2.25}$$

encountered in both objective function and constraints is the only non-linear component in the problems formulated in Section 3.1. As such, to a large extent it determines the computational complexity in solving these problems. An effective way to handle $l_\gamma(t, y)$ is to build a simple local model of the function at a given iterate (t_k, y_k). It turns out that $l_\gamma(t, y)$ always has a rank-1 Hessian, hence it admits a very simple convex quadratic model surrounding (t_k, y_k) as

$$l_\gamma(t, y) \approx l_\gamma(t_k, y_k) + \boldsymbol{g}_k^T\boldsymbol{\delta} + \frac{1}{2}(\boldsymbol{v}_k^T\boldsymbol{\delta})^2 \triangleq l_\gamma^{(k)}(t, y) \tag{2.26}$$

where $\boldsymbol{g}_k = \begin{bmatrix} -\log(1+\frac{\gamma y_k}{t_k}) + \frac{\gamma y_k}{t_k+\gamma y_k} \\ -\frac{\gamma t_k}{t_k+\gamma y_k} \end{bmatrix}$, $\boldsymbol{v}_k = \begin{bmatrix} \frac{\gamma y_k}{\sqrt{t_k}(t_k+\gamma y_k)} \\ -\frac{\gamma\sqrt{t_k}}{t_k+\gamma y_k} \end{bmatrix}$ and $\boldsymbol{\delta} = [t - t_k, y - y_k]^T$. Fig. 2.6 depicts the quadratic $l_\gamma^{(k)}(t, y)$ (the surface in black) in comparison with the original $l_\gamma(t, y)$ (the color surface) over a fairly large region $0.1 \leq t \leq 0.9$ and $0.01 \leq y \leq 0.1$

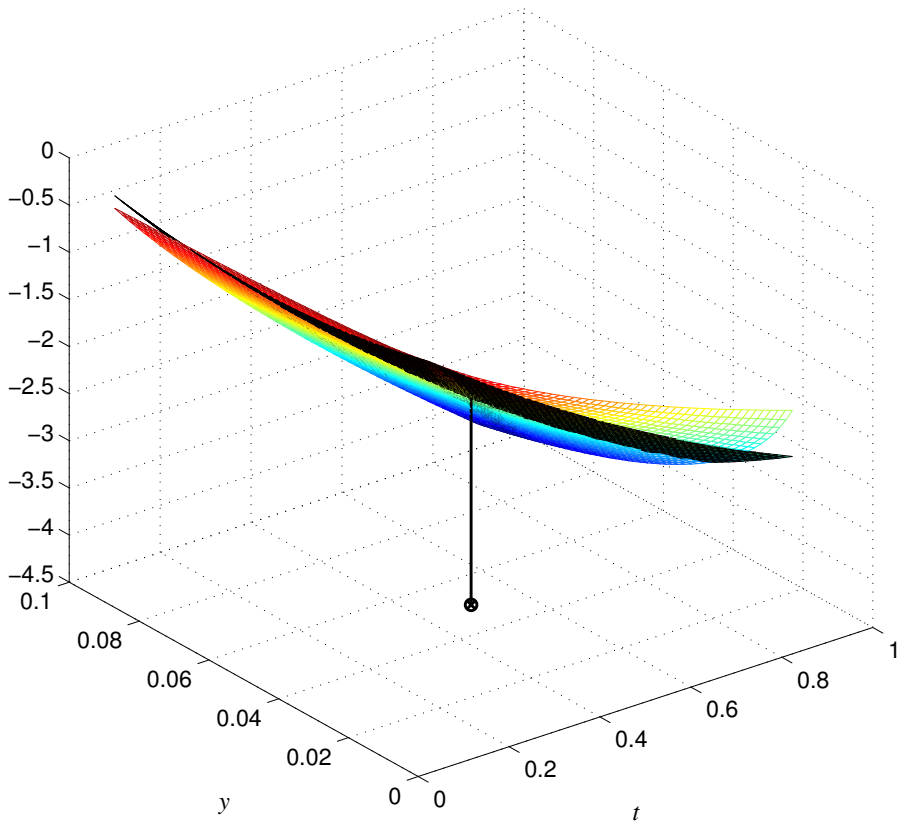

Figure 2.6: Perspective $l_\gamma(t, y)$ (the color surface) versus its quadratic approximation with (t_k, y_k) = (0.5, 0.05) and $\gamma = 1$ (the black surface).

with $t_k = 0.5$ and $y_k = 0.05$. Over this region, both $l_\gamma(t, y)$ and $l_\gamma^{(k)}(t, y)$ vary in the range [-4.2475,-0.4615], and the closeness between the two functions in terms of the normalized Frobenius norm of $l_\gamma(t, y) - l_\gamma^{(k)}(t, y)$ over 251×251 grid points of the region was found to be 0.07.

(2) Convex quadratic formulations

Based on (2.26), convex formulations are simplified counterparts of the problems formulated in Section 3.1 that are obtained by replacing all logarithmic perspective functions involved by quadratic approximation of the form in (2.26). For illustration, the local quadratic formulation of problem P1-A (see (2.17)) at iterate (t_k, y_k) is given by

$$(\text{P1}^{(k)}\text{-A}) \quad \underset{\boldsymbol{t},\boldsymbol{y},\boldsymbol{B}}{\text{maximize}} \quad -w_1 l_{\gamma_1}^{(k)}(t_1, y_1) + w_2 B \tag{2.27a}$$

$$\text{s.t.} \quad B \leq -l_{\gamma_2}^{(k)}(t_3, y_3) - l_{\gamma_1}^{(k)}(t_5, y_5) \tag{2.27b}$$

$$B \leq -l_{\gamma_u}^{(k)}(t_3, y_3) \tag{2.27c}$$

$$(2.17d) - (2.17j) \tag{2.27d}$$

The problem in (2.27) is a convex quadratically constrained quadratic programming (QCQP) problem. Based on (2.18) - (2.20), the quadratic approximation also applies to other scenarios, and QCQP formulations can be constrained for (P1-A), (P1-B), and (P2-B), and QP formulations can be obtained for (P3-A), (P3-B), (P4-A) and (P4-B). It will be shown later in Section 2.4, that the algorithm based on approximate QCQP is much faster than that based on the original problems.

2.4 Fast algorithms for optimal energy harvesting

Energy management and data transmission are supposed to be performed in real-time. As such, optimal strategies must be constructed fast enough for them to be useful. Reliable and efficient algorithms for constrained convex problems are available, yet the computer codes realizing these algorithms are not designed to take advantages offered by particular problem structures from a particular application. In this section, we first propose an enhanced *Newton barrier* algorithm that is tailored to solve the original problems formulated in Section 2.3.1. Newton methods are well known for fast convergence and high solution accuracy. They are especially suited because of the moderate problem sizes encountered here. A barrier term is incorporated to take care of the constraints and convert the problem at hand into an *unconstrained* convex problem. A line search technique is developed to take full advantage that each Newton direction has to offer so as to accelerate the algorithm considerably. Furthermore, as an alternative approach, we build an iterative algorithm for optimal EH based on the approximate quadratic formulations described in Section 2.3.2.

2.4.1 The Newton barrier (NB) algorithm for EH

(1) The algorithm

We consider problem P1-A as a representative formulation to illustrate the technical details of the proposed algorithm. With some notation simplified, P1-A is clearly equivalent to the following convex problem which we shall examine in the rest of Section 2.4.1:

$$\underset{\boldsymbol{t},\boldsymbol{y},B}{\text{minimize}} \quad f(\boldsymbol{x}) = -w_1 t_1 \log(1 + \gamma_1 \frac{y_1}{t_1}) - w_2 B \tag{2.28a}$$

Algorithm 1 Newton Barrier Algorithm

Input: Energy arrival rates $\{X_i\}$, SNRs $\{\gamma_i\}$, weights $\{w_i\}$, μ, initial point $\boldsymbol{x}_0$ and tolerance ϵ.

Output: Optimal solution $\boldsymbol{x}^*$.

Initialize all variables with strictly feasible points $n \leftarrow 0, \tau_n = \tau_0, \boldsymbol{x}_n^{(0)} \leftarrow \{\boldsymbol{B}_0, \boldsymbol{t}_0, \boldsymbol{y}_0\}$.
while $||\boldsymbol{x}_n - \boldsymbol{x}_{n-1}||_2 > \epsilon$ **do**
    Initialize $k \leftarrow 0, \boldsymbol{x}_k = \boldsymbol{x}_n^{(0)}$
    while $||\boldsymbol{x}_k - \boldsymbol{x}_{k-1}||_2 > \epsilon$ **do**
        Compute gradient $\boldsymbol{g}_k$ of $F_\tau(\boldsymbol{x}_k)$ and Hessian $\boldsymbol{H}_k$ of $F_\tau(\boldsymbol{x}_k)$.
        Compute search direction $\boldsymbol{d}_k \leftarrow -\boldsymbol{H}_k^{-1}\boldsymbol{g}_k$.
        Find a step size α_k that minimizes $f(\boldsymbol{x}_k + \alpha \boldsymbol{d}_k)$ subject to (2.28b) - (2.28h).
        $\boldsymbol{x}_{k+1} \leftarrow \boldsymbol{x}_k + \alpha_k \boldsymbol{d}_k$, $k \leftarrow k+1$.
    end while
    $\boldsymbol{x}_{n+1}^{(0)} \leftarrow \boldsymbol{x}_k^*$, $\tau_{n+1} \leftarrow \mu\tau_n$, $n \leftarrow n+1$.
end while
$\boldsymbol{x}^* \leftarrow \boldsymbol{x}_n$

$$\text{s.t.} \quad c_1(\boldsymbol{x}) = B - t_3 \log(1+\gamma_2 \frac{y_3}{t_3}) - t_5 \log(1+\gamma_1 \frac{y_5}{t_5}) \leq 0 \tag{2.28b}$$

$$c_2(\boldsymbol{x}) = B - t_3 \log(1+\gamma_u \frac{y_3}{t_3}) \leq 0 \tag{2.28c}$$

$$c_3(\boldsymbol{x}) = y_1 - X_1(1-t_1-t_2-t_3-t_4-t_5) \leq 0 \tag{2.28d}$$

$$c_4(\boldsymbol{x}) = y_1 + y_2 - X_1(1-t_2-t_3-t_4-t_5) \leq 0 \tag{2.28e}$$

$$c_5(\boldsymbol{x}) = -\beta y_2 + y_3 - X_2(1-t_3-t_4-t_5) \leq 0 \tag{2.28f}$$

$$c_6(\boldsymbol{x}) = -\beta y_2 + y_3 + y_4 - X_2(1-t_4-t_5) \leq 0 \tag{2.28g}$$

$$c_7(\boldsymbol{x}) = y_1 + y_2 - \beta y_4 + y_5 - X_1(1-t_5) \leq 0 \tag{2.28h}$$

$$c_8(\boldsymbol{x}) = t_1 + t_2 + t_3 + t_4 + t_5 - 1 \leq 0 \tag{2.28i}$$

$$t_i \geq 0, y_i \geq 0, i = 1,2,3,4,5 \tag{2.28j}$$

where $B = B_{2A}, \beta = \eta h_u$, and $\boldsymbol{x} = [\boldsymbol{t}, \boldsymbol{y}, B]$.

The NB algorithm solves (2.28) by iteratively solving the unconstrained problem

$$\text{minimize} \quad F_\tau(\boldsymbol{x}) = -w_1 t_1 \log(1+\gamma_1 \frac{y_1}{t_1}) - w_2 B - \frac{1}{\tau}(\sum_{j=1}^{8} \log(-c_j(\boldsymbol{x})) + \sum_{i=1}^{5} \log(t_i) + \log(y_i)) \tag{2.29}$$

where $\tau > 0$ is a barrier parameter that increases as the iteration proceeds so that minimizing $F_\tau(\boldsymbol{x})$ gradually becomes the same as minimizing the original objective function

in (2.28), yet the presence of the logarithmic barrier term in (2.29) assures that the iterates produced remain strictly inside the feasible region defined by (2.28b) - (2.28j). The algorithm starts with a strictly feasible initial $\boldsymbol{x}_0$ and an initial $\tau = \tau_0 > 0$. Newton algorithm is applied to minimize $F_{\tau_0}(\boldsymbol{x})$ and its solution is in turn used to initiate the next minimization of $F_{\tau_1}(\boldsymbol{x})$ where $\tau_1 = \mu\tau_0$ with μ a constant factor, say $\mu = 10$, to yield a larger τ_1. The iteration continues until the 2-norm difference between two consecutive iterates is less than a prescribed tolerance ϵ.

For a fixed τ, the Newton step assumes the form

$$\boldsymbol{x}_{k+1} = \boldsymbol{x}_k + \alpha_k \boldsymbol{d}_k \tag{2.30a}$$

$$\boldsymbol{d}_k = -(\nabla^2 F_\tau(\boldsymbol{x}_k))^{-1} \nabla F_\tau(\boldsymbol{x}_k) \tag{2.30b}$$

where α_k minimizes $f(\boldsymbol{x}_k + \alpha_k \boldsymbol{d}_k)$ subject to constraints (2.28b) - (2.28h).

A technique for fast identification of α_k is described in part (2) of this section. The proposed method is summarized in Algorithm 1.

(2) A line search technique for optimal α_k^*

The line search that finds a step size α_k to minimize $f(\boldsymbol{x}_k + \alpha \boldsymbol{d}_k)$ for given $\boldsymbol{x}_k$ and $\boldsymbol{d}_k$ consists of three steps. Denote $\boldsymbol{x}_k = [\boldsymbol{t}_k, \boldsymbol{y}_k, B_k]$ that strictly satisfies constraints (2.28b) - (2.28h), and $\boldsymbol{d}_k$ obtained from (2.30b) as $\boldsymbol{d}_k = [\boldsymbol{\delta}_t, \boldsymbol{\delta}_y, \delta_B]$ with $\boldsymbol{\delta}_t = [\delta_{t_1}, \delta_{t_2}, \delta_{t_3}, \delta_{t_4}, \delta_{t_5}]$ and $\boldsymbol{\delta}_y = [\delta_{y_1}, \delta_{y_2}, \delta_{y_3}, \delta_{y_4}, \delta_{y_5}]$. The first step of the line search determines an interval of α, $[0, \alpha_I]$, over which $\boldsymbol{x}_k + \alpha \boldsymbol{d}_k$ satisfies the linear constraints (2.28d) - (2.28j). The value of such α_I can be found by simply finding the largest α_j such that $c_j(\boldsymbol{x}_k + \alpha \boldsymbol{d}_k) < 0$ over $[0, \alpha_j]$ for $3 \le j \le 8$; then the largest $\hat{\alpha}$ that over $[0, \hat{\alpha}]$, $\boldsymbol{x}_k + \alpha \boldsymbol{d}_k$ satisfies (2.28h). Because of the linearity of these constraints, it can be readily verified that

$$\alpha_3 = \begin{cases} +\infty & \text{if } q_3 = -X_1(\delta_{t_1} + \delta_{t_2} + \delta_{t_3} + \delta_{t_4} + \delta_{t_5}) - \delta_{y_1} \ge 0 \\ \frac{c_3(\boldsymbol{x}_k)}{q_3} & \text{otherwise} \end{cases} \tag{2.31a}$$

$$\alpha_4 = \begin{cases} +\infty & \text{if } q_4 = -X_1(\delta_{t_2} + \delta_{t_3} + \delta_{t_4} + \delta_{t_5}) - \delta_{y_1} - \delta_{y_2} \ge 0 \\ \frac{c_4(\boldsymbol{x}_k)}{q_4} & \text{otherwise} \end{cases} \tag{2.31b}$$

$$\alpha_5 = \begin{cases} +\infty & \text{if } q_4 = -X_2(\delta_{t_3} + \delta_{t_4} + \delta_{t_5}) + \beta\delta_{y_2} - \delta_{y_3} \ge 0 \\ \frac{c_5(\boldsymbol{x}_k)}{q_5} & \text{otherwise} \end{cases} \tag{2.31c}$$

$$\alpha_6 = \begin{cases} +\infty & \text{if } q_6 = -X_2(\delta_{t_4} + \delta_{t_5}) + \beta\delta_{y_2} - \delta_{y_3} - \delta_{y_4} \ge 0 \\ \frac{c_7(\boldsymbol{x}_k)}{q_7} & \text{otherwise} \end{cases} \tag{2.31d}$$

$$\alpha_7 = \begin{cases} +\infty & \text{if } q_7 = -X_1\delta_{t_5} - \delta_{y_1} - \delta_{y_2} + \beta\delta_{y_4} - \delta_{y_5} \geq 0 \\ \frac{c_7(\boldsymbol{x}_k)}{q_7} & \text{otherwise} \end{cases} \tag{2.31e}$$

$$\alpha_8 = \begin{cases} +\infty & \text{if } q_8 = \delta_{t_1} + \delta_{t_2} + \delta_{t_3} + \delta_{t_4} + \delta_{t_5} \geq 0 \\ \frac{c_8(\boldsymbol{x}_k)}{q_8} & \text{otherwise} \end{cases} \tag{2.31f}$$

$$\hat{\alpha} = \min\{-\frac{t_i}{\delta_{t_i}}_{\delta_{t_i}<0}, -\frac{y_i}{\delta_{y_i}}_{\delta_{y_i}<0}, +\infty\}. \tag{2.31g}$$

It follows that

$$\alpha_I = 0.99 \min\{\alpha_3, \alpha_4, \alpha_5, \alpha_6, \alpha_7, \alpha_8, \hat{\alpha}\} \tag{2.32}$$

where the scaling factor 0.99 assures strict feasibility of $\boldsymbol{x}_k + \alpha\boldsymbol{d}_k$ on $[0, \alpha_I]$ for (2.28d) - (2.28h).

Next, we identify the largest subinterval $[0, \alpha_{II}]$ of $[0, \alpha_I]$, where $\boldsymbol{x}_k + \alpha\boldsymbol{d}_k$ is strictly feasible for constraints (2.28b) and (2.28c). Note that over $[0, \alpha_I]$ the logarithmic terms in (2.28b) and (2.28c) are well defined because the first six components of $\boldsymbol{x}_k + \alpha\boldsymbol{d}_k$ (that are the t and y components) remain strictly positive due to (2.28h). Also note that both $c_1(\boldsymbol{x}_k + \alpha\boldsymbol{d}_k)$ and $c_2(\boldsymbol{x}_k + \alpha\boldsymbol{d}_k)$ are convex functions of α over $[0, \alpha_I]$. This in conjunction with the fact that both $c_1(\boldsymbol{x}_k)$ and $c_2(\boldsymbol{x}_k)$ are strictly negative (because $\boldsymbol{x}_k$ is a strictly feasible iterate) implies that $c_1(\boldsymbol{x}_k + \alpha\boldsymbol{d}_k)$ and $c_2(\boldsymbol{x}_k + \alpha\boldsymbol{d}_k)$ each has at most one zero crossing over $[0, \alpha_I]$ and the zero crossings, denoted by $\alpha^{(1)}$ and $\alpha^{(2)}$ for $c_1(\boldsymbol{x}_k)$ and $c_2(\boldsymbol{x}_k)$, respectively, can be identified by standard bisection which checks the sign of the function at the mid-point of the interval to decide which part of the interval to keep in order to proceed the bisection procedure. Evidently, $\alpha_{II} = 0.99 \min\{\alpha^{(1)}, \alpha^{(2)}\}$ assures that both $c_1(\boldsymbol{x}_k + \alpha\boldsymbol{d}_k)$ and $c_2(\boldsymbol{x}_k + \alpha\boldsymbol{d}_k)$ remain strictly feasible for α over $[0, \alpha_{II}]$.

The final step of the line search looks for a minimizer of the objective function $f(\boldsymbol{x}_k + \alpha\boldsymbol{d}_k)$ in (2.28a) as a function of α over $[0, \alpha_{II}]$. Because $f(\boldsymbol{x}_k + \alpha\boldsymbol{d}_k)$ is convex with respect to α, it has a unique minimizer over $[0, \alpha_{II}]$, and the minimizer, denoted by α_k, can readily be identified using, for example, the golden-section method that only requires a small number of evaluations of the objective function [48].

2.4.2 An iterative algorithm based on local quadratic formulations

For illustration purpose we consider the problem in (2.27), which we call P1$^{(k)}$-A as it is obtained through quadratic approximation of the logarithmic perspective functions involved in P1-A and the formulation is valid in a vicinity of the kth iterate (t_k, y_k).

With a strictly feasible initial point $\boldsymbol{x}_0$, the proposed algorithm calls a convex programming (CP) solver to solve the convex QCQP subproblem P1$^{(0)}$-A as formulated in (2.27) for a global solution denoted as $\boldsymbol{x}_0^*$. This $\boldsymbol{x}_0^*$ serves as an initial point for the next iteration in that the quadratic approximation is carried out at $\boldsymbol{x}_0^*$ and the updated QCQP subproblem is solved to obtain iterate $\boldsymbol{x}_1^*$. The iteration continues until $||\boldsymbol{x}_k - \boldsymbol{x}_{k-1}||_2$ falls below a prescribed tolerance ϵ.

The reader is referred to Algorithm 2 for a step-by-step outline of this iterative approach. Our numerical experiments have demonstrated that Algorithm 2 converges within a small number (typically in less than 10) iterations. Therefore, the complexity of Algorithm 2 is largely determined by the complexity of the QCQP subproblem. We have developed an interior-point path-following primal-dual algorithm which is tailored to the structure of problem (2.27) with a closed-form exact line search step. The customized MATLAB code implementing the above algorithm was evaluated in comparison with a CVX-based counterpart, and the average CPU time required by our code was found in the range 0.0086 to 0.01 normalized time units versus 1 time unit by the CVX-based code. Note that the programs are all run on a MacBook Pro with 2.7 GHz Intel Core i5 processor and 8 GB 1867 MHz DDR3 memory.

We remark that Step 3 of Algorithm 2 where a CP solver is called to solve a QCQP subproblem will have to be modified to solve a QP subproblem when scenarios P3 and P4 are examined. The QP subproblem can be solved by an efficient interior-point algorithm [48]. Comparisons of average CPU time required by several available computer code are illustrated in Table 2.5 where the average CPU required by MATLAB function $\mathrm{fmincon}$ was normalized to one unit.

Algorithm 2 An iterative algorithm based on local quadratic formulations

Input: Energy arrival rates $\{X_i\}$, SNRs $\{\gamma_i\}$, PS ratio ρ, weights $\{w_i\}$ and tolerance ϵ.
Output: Optimal solution $\boldsymbol{x}^*$.

1: Initialize all variables with strictly feasible points $k \leftarrow 0, \boldsymbol{x}_0^* \leftarrow \{\boldsymbol{B}_0, \boldsymbol{t}_0, \boldsymbol{y}_0\}, \mathrm{dif}_0 > \epsilon$.
2: **while** $\mathrm{dif}_k > \epsilon$ **do**
3: Use $\boldsymbol{x}_k^*$ to initiate a CP solver for P1$^{(k)}$-A in (2.27). Denote the solution obtained by $\boldsymbol{x}_{k+1}^*$.
4: $\mathrm{dif}_k = ||\boldsymbol{x}_{k+1}^* - \boldsymbol{x}_k^*||_2, k \leftarrow k + 1$.
5: **end while**
6: $\boldsymbol{x}^* \leftarrow \boldsymbol{x}_k^*$

Table 2.5: Comparisons of Average CPU Time Ratio where Average CPU Time Required by MATLAB Function FMINCON was Normalized to 1 Unit

	Our proposed methods			**Other available methods**		
	original model	**approximate model**		**original model**		**approximate model**
	NB	**QCQP**	**QP**	**fmincon**	**CVX**	**quadpro**
P1-A	0.5517	0.4917	–	1	55.25	–
P3-A	0.0294	–	0.2169	1	60.24	3.602

2.5 Numerical Results

In the numerical study reported below, the path loss exponent was set to $a = 2$ and the average signal power attenuation at a reference of 1 unit of distance was set to 30dB, hence channel gain $h_i = 10^{-3} d_i^{-2}$ for $i = 1, 2, u$, where d_u denotes the distance between U_1 and U_2. All receiver noise power density was set to -160 dBm/Hz and the bandwidth was set to 1 MHz. The energy conversion efficiency $\eta = 0.75$ [25]. The weights of two users were set to be equal as $w_1 = w_2 = 1$. Through numerical study, the optimal strategy that employs EC or DC or both is searched for different channel conditions and energy harvesting environments in a three-node setup. For illustration purpose, the three nodes are assumed to be positioned on one line.

2.5.1 Performances of Case A versus energy arrival rate of U_2

In this part of numerical study, the distance between U_1 and D and distance between U_1 and U_2 were set to $d_1 = 1$ (unit), and the distance between U_2 and D was $d_2 = 2$.

When $X_1 \gg X_2$, Case A is employed hence U_1 can share energy with U_2. By fixing the energy arrival rate $X_1 = 2000$ mW (millijoule per unit of time), the maximum sum-throughputs and common-throughputs in S1-A to S4-A when X_2 increases from 0 to 1 mW are compared and shown in Fig. 2.7. It is observed in Fig. 2.7(a) that when $X_1 \gg X_2$, four maximum sum-throughputs in Case A are pretty close to each other, compared with four maximum common-throughputs in common-throughput maximization. It is because when X_2 is extremely small, sum-throughput maximization strategy allocates most resources to U_1 and throughput of U_2 is nearly zero. On the other hand, common-throughput maximization is illustrated in Fig. 2.7(b). When $X_2 = 0$, common-throughputs of U_1 and U_2 in S2-A and S4-A are restricted by U_2. However, in S1-A and S3-A, U_1 shares its energy to U_2 before U_2 transmits. Therefore, the common-throughputs of U_1 and U_2 are improved. When X_2 increases from 0 to 1 mW, S1-A is seen as the best strategy employing both en-

ergy cooperation and data cooperation, and S3-A is the second best. Both S1-A and S3-A include EC strategies, which is in agreement with our analysis.

2.5.2 Performances of Case B versus energy arrival rate of U_1

In this part of numerical study, the distance between U_1 and D and distance between U_1 and U_2 were also set to $d_1 = 1$ (unit), and again the distance between U_2 and D was $d_2 = 2$.

When $X_2 \gg X_1$, Case B is employed so that U_2 can share energy to U_1. By fixing the energy arrival rate $X_2 = 2000$ mW (millijoule per unit of time), the maximum sum-throughputs and common-throughputs in S1-B to S4-B when X_1 increases from 0 to 1 mW are compared and shown in Fig. 2.8. We observe in Fig. 2.8(a) and Fig. 2.8(b) that when $X_2 \gg X_1$, the maximum sum-throughputs and common-throughputs in S1-B and S3-B are pretty close to each other, while the results from S2-B are close to those in S4-B. Similarly, when $X_1 = 0$, the common-throughputs of U_1 and U_2 in S2-B and S4-B are zero because of U_1. In contrast, the common-throughputs of U_1 and U_2 are enhanced by energy sharing from U_2 in S1-B and S3-B.

In summary, when X_2 increases from 0 to 1mW, S1-B and S3-B strategies employing EC perform better than S2-B and S4-B, which is in agreement with the results obtained in case A.

2.5.3 Performance versus distance from U_1 to D in case A

In this part of numerical study, performance in S1-A - S4-A versus changing distance from U_1 to D is analyzed. Energy arrival rate of U_1 was fixed to 2000 mW ($X_1 = 2000mW$) and X_2 was fixed to 0.5 mW. U_1, U_2 and D were located in a line, i.e., $d_u = d_2 - d_1$. In addition, the distance between U_2 and D was fixed to $d_2 = 2$, and d_1 varies incrementally from 0.2 to 1.8.

The results obtained are shown in Fig. 2.9 where optimal sum-throughputs versus distance from U_1 to D are compared with the common-throughput obtained by common-throughput maximization. It can be observed that four trajectories of sum-throughputs almost coincide with each other when U_1 is far from U_2 ($d_1 < 1.4$, $d_u > 0.6$). In addition, with d_1 increasing from 0.2 to 1.4, the sum-throughputs in S1-A - S4-A are decreasing. However, if two users are close enough, the sum-throughputs in S1-A and S3-A with EC begin to rise at $d_1 = 1.6$ ($d_u = 0.4$). On the other hand, the common-throughputs in S1-A and S3-A with EC begin to rise at $d_1 = 0.6$ ($d_u = 2.4$), much earlier than that in sum-throughput maximization. And both sum-throughputs and common-throughputs in S4-A

with neither EC nor DC are decreasing throughout. This is because when two users get closer, the channel condition between the two users improves, which helps increase the both energy harvested from the other user according to (2.1b) and the quality of relay forwarding. In summary, EC strategies are shown to be more adaptive to distance changing relative to DC, and we see that among the four scenarios S1-A performs the best in both sum-throughput maximization and common-throughput maximization due to the advantages of both EC and DC, while without any cooperation S4 performs the worst.

Numerical results of optimal individual throughputs achieved by sum-throughput maximization with the common-throughput from common-throughput maximization in S1-A are shown in Fig. 2.10. It can be observed that the throughput of U_1 is decreasing while the throughput of U_2 is increasing when two users are getting close. Even though U_2 is lack of natural energy, it is surprisingly found that the throughput of U_2 approaches to U_1 when $d_1 = 1.8$ ($d_u = 0.2$) due to energy sharing and data cooperation.

The above analysis demonstrates that when there is a disparity between energy arrival rates of two users, i.e., $X_1 \gg X_2$ or $X_2 \gg X_1$, the use of EC strategies leads to rather remarkable improvement in system performance. We also observe that EC and DC strategies become more effective when two user nodes are sufficiently close.

2.6 Summary

In this chapter, we have proposed an adaptive cooperative wireless communication network strategy with energy cooperation (EC) and data cooperation (DC) techniques. Taking into account the transmission order of two users in a three-node network, optimal energy management strategies are investigated in terms of maximal weighted sum-throughput or minimum throughput of the two users for four possible scenarios. An accelerated Newton barrier algorithm and an alternative algorithm based on local quadratic approximation of the transmission models are developed to solve the proposed optimization problems. Numerical results have shown that employing EC and DC strategies does help to enhance the performance of the system.

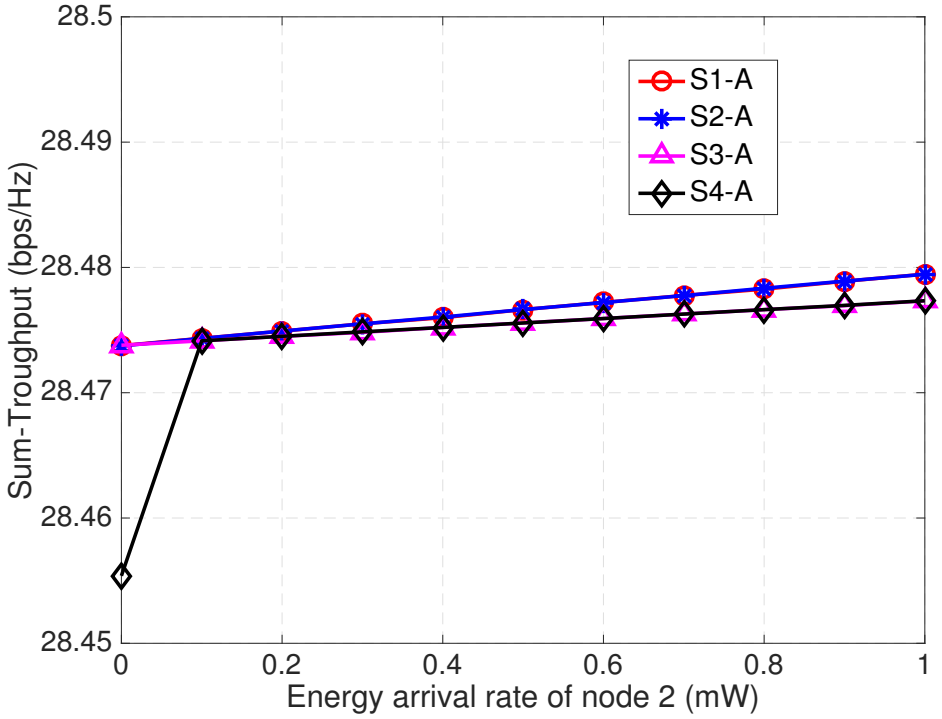

(a) Sum-throughput

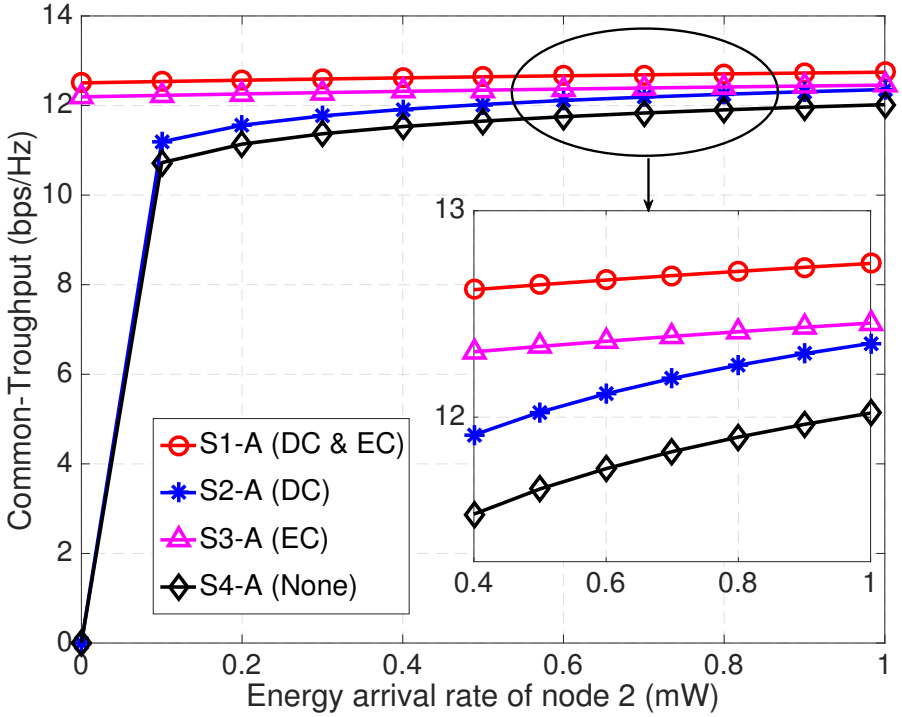

(b) Common-throughput

Figure 2.7: Sum-throughput and common-throughput maximization in S1-A - S4-A with X_1 fixed to 2000 mW.

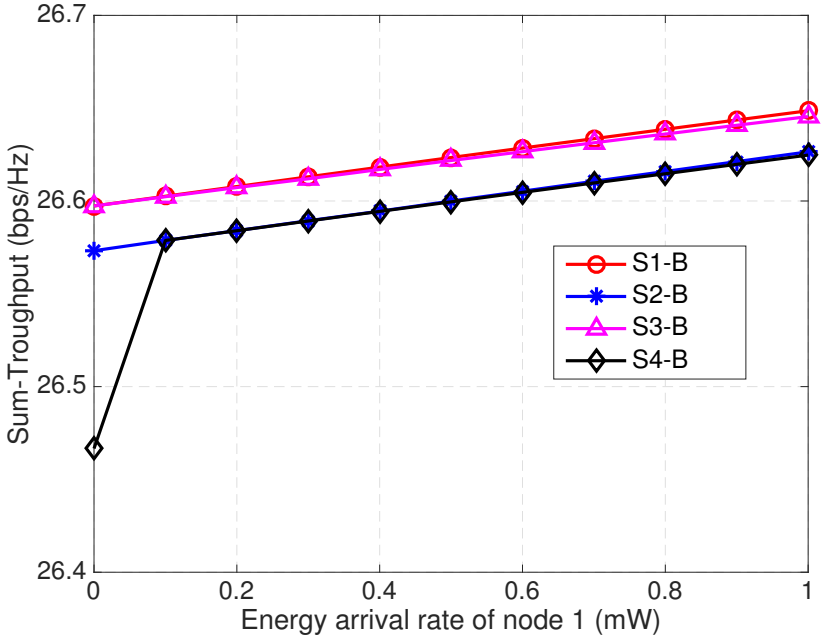

(a) Sum-throughput

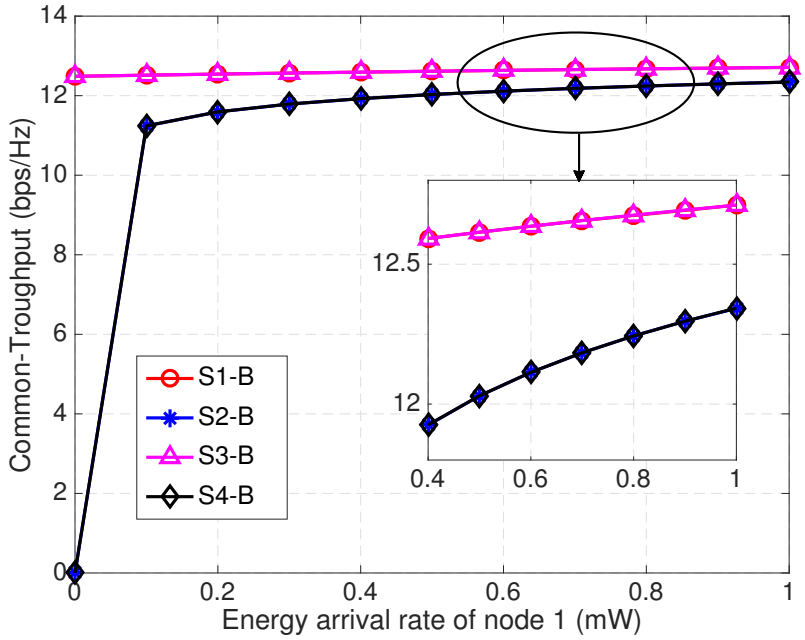

(b) Common-throughput

Figure 2.8: Sum-throughput and common-throughput maximization in S1-B - S4-B with X_2 fixed to 2000 mW.

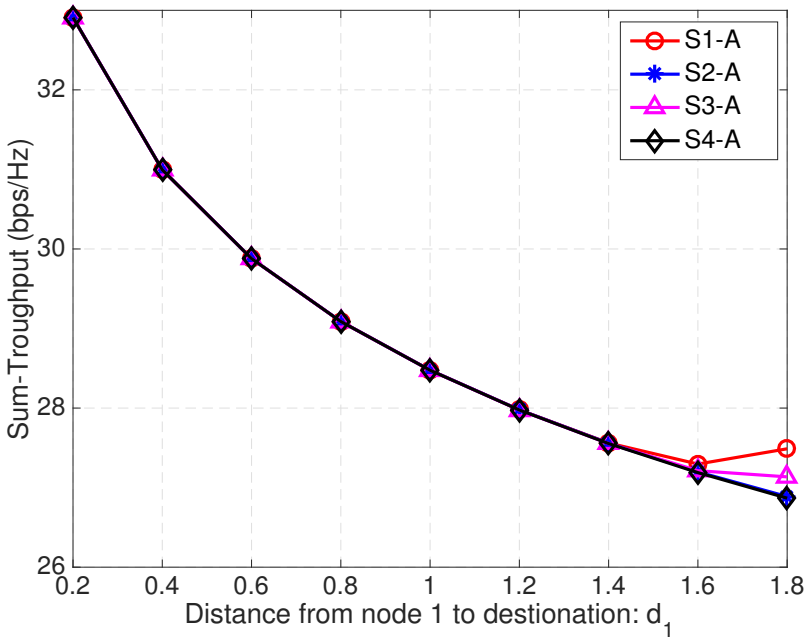

(a) Equal-weighted sum-throughput maximization

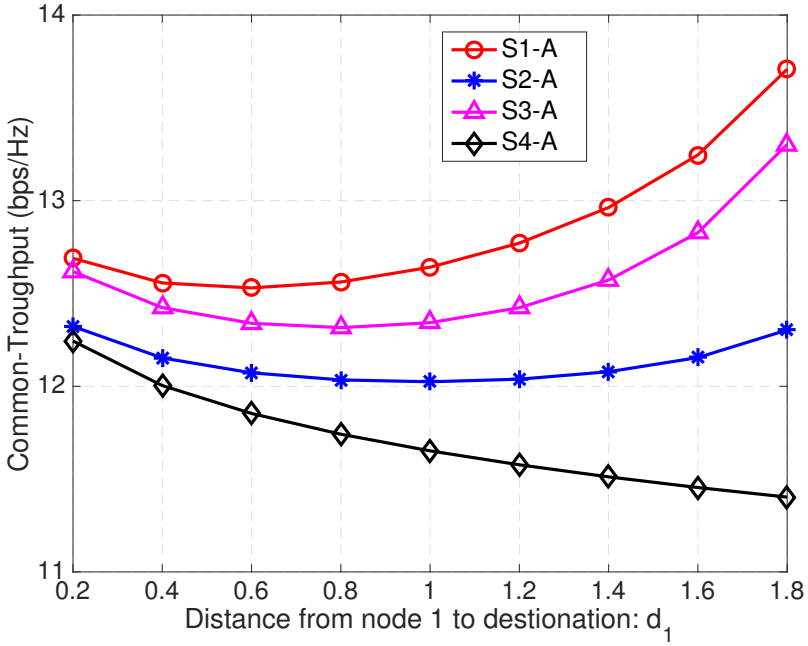

(b) Common-throughput maximization

Figure 2.9: Comparisons of (a) equal-weighted sum-throughput maximization and (b) common-throughput maximization in S1-A - S4-A versus distance from U_1 to D.

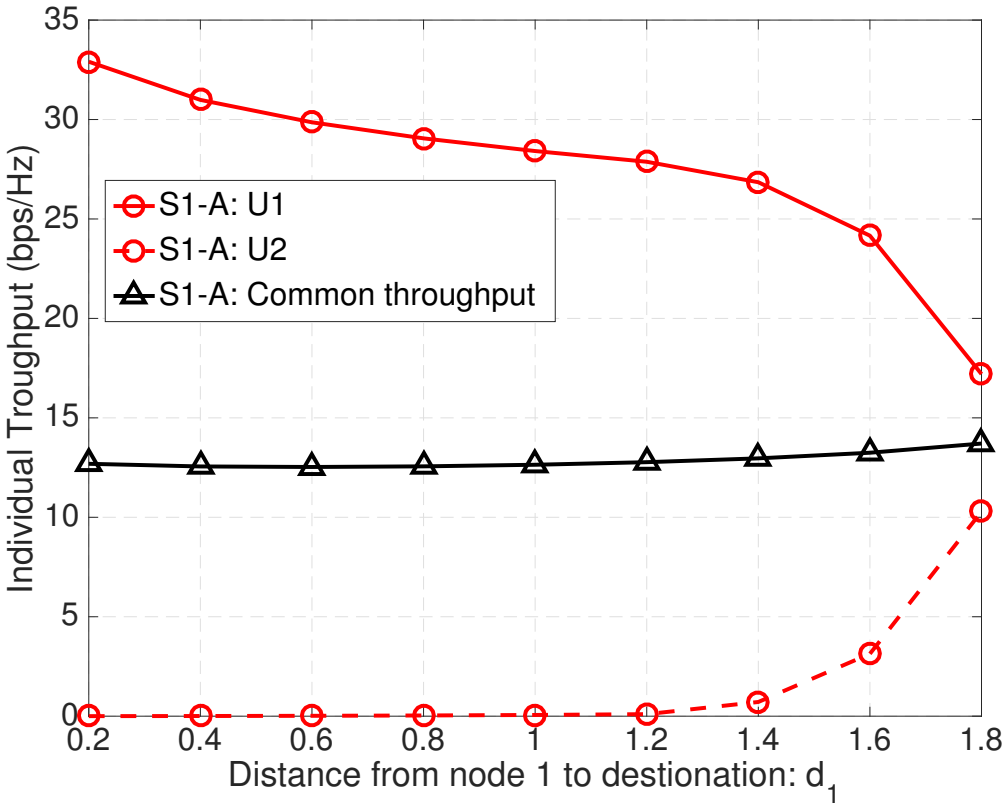

Figure 2.10: Comparisons of optimal individual throughputs by sum-throughput maximization and the common-throughput by common-throughput maximization in S1-A with X_1 fixed to 0.5 mW and X_2 fixed to 2000 mW.

Chapter 3

Optimal Energy Management Strategies in Wireless Energy Harvesting Communications with Multiple Users

3.1 Introduction

Recently, energy harvesting (EH) from ambient radio frequency (RF) signals has been a promising solution to prolong the lifetime of wireless communication networks [1,13]. One important EH research direction is simultaneous wireless information and power transfer (SWIPT) via RF signals [2]. To characterize the fundamental tradeoff between simultaneous data transmission and energy harvesting, a capacity-energy function is defined in [15]. Moreover, a rate-energy (R-E) region for a multiple-input multi-output wireless system is characterized in [16], where two practical receiver schemes, known as time switching (TS) and power splitting (PS), are proposed so that EH and information decoding (ID) are operated independently. The achievable R-E region with SWIPT techniques is also studied under the proposed dynamic PS scheme in [35].

With the rapid development of SWIPT techniques, researchers are interested in optimizing the performance of wireless EH communication networks via cooperative relay assisted system [38, 41, 43, 45, 49, 50]. In [38], the proposed cooperative transmission protocols enable the relay node to forward the source's information and the source to harvest energy from the relay's transmission signals. Two different relay protocols based on TS and PS techniques to separate EH and ID parts are proposed in [41], where an relay node replenishes energy from the received RF signal transmitted by the source node. In [43], an EH

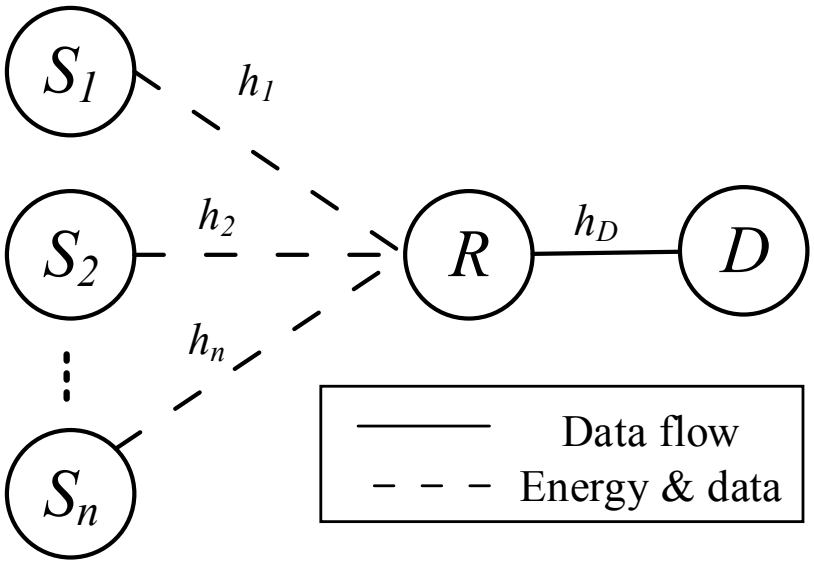

Figure 3.1: System model for a cooperative multi-user network with relay assistance.

relay employs PS to harvest energy from RF signals transmitted by multiple sources, and then forwards information to multiple associated destinations. On the other hand, in [49], tradeoffs between the quality of data transmission and total amount of harvested energy are investigated under different relay selection policies with multiple EH relays. In [45], the near user to the hybrid access point, selected as the "relay" node, transmits its own data first and then forwards the information of the "far" user. Furthermore, in [50], throughput analysis is investigated based on two TS modes for the EH duration time of the relay, continuous time EH and discrete time EH, where both amplify-and-forward (AF) and decode-and-forward (DF) relaying protocols are considered. Considering both data and energy cooperation in Chapter 2, optimal energy management strategies are studied based on a new cooperative EH protocol adaptive to the energy harvesting and propagation environments.

Prior works focus on a simple relay system model with only one source [38, 41, 45, 49, 50]. In this chapter, we are motivated to study in a multi-source network with relay assistance as shown in Fig. 3.1. We assume that N source nodes $S_1, S_2 \dots S_N$ transmit their individual messages via an EH relay R through time-division multiple access (TDMA). In addition, the power-splitting strategy is employed that allows the relay to replenish energy from the RF signals transmitted by the sources, and then forwards the information from each source to the destination D through TDMA. In this chapter, DF relaying is considered and the relay has no other energy supply. Based on the proposed protocol, the convex prob-

lems of characterizing the *Energy-Throughput* (E-T) tradeoffs between maximal amount of saved energy and achievable average throughput are formulated. When there is only one source node, the closed-form solution is derived by solving Karush-Kuhn-Tucker (KKT) conditions. When there are multiple source nodes, we propose two strategies: one is common PS ratio strategy that the relay adopts the same PS ratio for all sources; the other is individual PS ratio strategy that each source uses an individual optimal PS ratio for the performance. We adopt the Newton Barrier algorithm in Section 2.3 and 2.4 to obtain the solutions of the associated multi-source convex problems.

The rest of the chapter is organized as follows. Section 3.2 presents the system model and transmission protocols. Section 3.3 presents E-T tradeoffs and a corresponding convex problem for the one-source scenario. In Section 3.4, E-T tradeoffs for both common PS ratio and individual PS ratio strategies are analyzed in multi-source scenarios. Numerical study and useful observations are provided in Section 3.5.

3.2 System model

As illustrated in Fig. 3.1, we consider a multi-source network with N source nodes $S_i, i = 1, 2, \ldots N$, an EH relay R and a destination D, each is equipped with an antenna. All source nodes transmit their own messages via the relay R through different time intervals, and there is no direct communication between sources and D.

Each channel in the network is characterized with a complex random variable $\tilde{h}$ with channel power gain $h = |\tilde{h}|^2$, which only considers distance-dependent path loss effects for simplicity. In doing so, the channel power gain is modeled as $h = \lambda d^{-\alpha}$, where d is the distance from the transmitter to the receiver, α an path-loss exponent and λ an average signal power attenuation at a reference of 1 unit of distance. In this section, we use $h_i = |\tilde{h}_i|^2$ and $h_D = |\tilde{h}_D|^2$ to denote the power gain of the channel from the user S_i to R and the power gain of the channel from R to D, respectively, with d_i and d_D to denote the distance from S_i to R, and R to D, respectively. All channels in our system model are assumed quasi-static block-fading, thus the channel gains remain constant during each transmission block T, but may vary from one block to another. For convenience, $T = 1$ unit of time is assumed in the rest of the section.

During the first phase of length $\frac{T}{2} = \frac{1}{2}$, each source node S_i transmits RF signals with constant transmission power P to the relay within an equal time duration of length $\frac{1}{2N}$, respectively. We model the complex baseband signal transmitted by S_i as s_i with

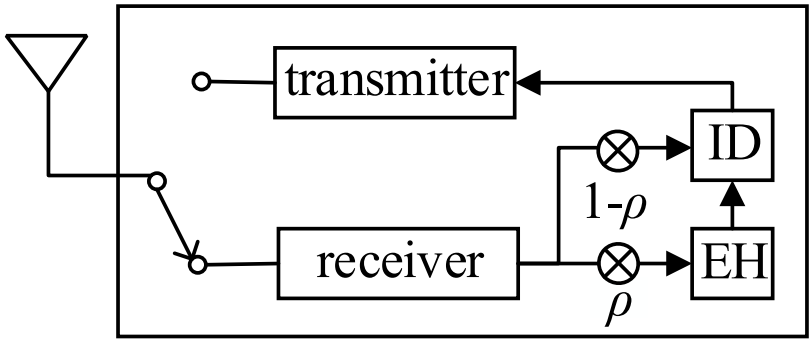

Figure 3.2: Energy harvesting and information decoding inside the relay node.

$\mathbb{E}[|s_i|^2] = P$, which is received by R as $y_{r,i}$

$$y_{r,i} = \sqrt{h_i} s_i + z_{ri} \tag{3.1}$$

with noise terms $z_{ri} \sim \mathcal{CN}(0, \sigma_r^2)$ at R.

At the end of the first phase, the relay uses PS technique [16] to split received RF signals from each source S_i into two parts: $\rho_i P$ with $0 \leq \rho_i \leq 1$ for EH as its energy supply, and the rest $(1 - \rho_i)P$ for ID as shown in Fig. 3.2, where the decode-and-forward strategy is considered. In such case, the amount of harvested energy from each source S_i at R, denoted by E_i, is expressed as

$$E_i = \frac{1}{2N} \eta \rho_i P h_i \tag{3.2}$$

where η is the energy harvesting efficiency.

During the second phase of length $\frac{1}{2}$, the relay forwards decoded data of each source to D within an equal time duration of length $\frac{1}{2N}$ respectively. Let x_i denote the complex baseband signal for source S_i transmitted by R with transmission power Q_i, hence $\mathbb{E}[|x_i|^2] = Q_i$. The corresponding received signals at D can be expressed as

$$y_{d,i} = \sqrt{h_d} x_i + z_{di} \tag{3.3}$$

with noise terms $z_{di} \sim \mathcal{CN}(0, \sigma_d^2)$ at D. At the end of the second phase, we have energy constraint

$$\frac{1}{2N} \sum_{i=1}^{N} \eta \rho_i P h_i \geq \frac{1}{2N} \sum_{i=1}^{N} Q_i \tag{3.4}$$

imposed on R. If the harvested energy is not used up, we have saved E_s amount of energy

$$E_s = \frac{1}{2N}\sum_{i=1}^{N}\eta\rho_i P h_i - \frac{1}{2N}\sum_{i=1}^{N} Q_i. \tag{3.5}$$

For every transmission block T, the amount of data throughput achievable by each source node S_i, and the amounts of data throughput achievable from S_i to R and from R to D are given by

$$B_i = \min[B_{sr}^i, B_{rd}^i] \tag{3.6a}$$

$$B_{sr}^i = \frac{1}{2N}\log_2(1 + \frac{(1-\rho_i)Ph_i}{\sigma_r^2}) = \frac{1}{2N}\log_2(1 + \bar{\rho}_i P\gamma_i) \tag{3.6b}$$

$$B_{rd}^i = \frac{1}{2N}\log_2(1 + \frac{Q_i h_d}{\sigma_d^2}) = \frac{1}{2N}\log_2(1 + Q_i\gamma_d) \tag{3.6c}$$

respectively, where $\gamma_i = \frac{h_i}{\sigma_r^2}$, $\gamma_d = \frac{h_d}{\sigma_d^2}$, and $\bar{\rho}_i = 1 - \rho_i$ [46].

3.3 Throughput and Energy Tradeoffs in one-source scenario

In this section, we investigate the tradeoffs between the amount of saved energy E_s at the relay and achievable average throughput of all source nodes τ, which is characterized by the boundary of *Energy-Throughput* (E-T) region $\mathcal{C}_{E-T}$ below [35]

$$\mathcal{C}_{E-T}(\boldsymbol{Q}, \boldsymbol{\rho}) \triangleq \{(E_s, \tau) : E_s \leq \frac{1}{2N}\sum_{i=1}^{N}\eta\rho_i P h_i - \frac{1}{2N}\sum_{i=1}^{N} Q_i, \tau \leq \frac{1}{N}\sum_{i=1}^{N} B_i\} \tag{3.7}$$

where transmission power vector is $\boldsymbol{Q} = [Q_1, \ldots, Q_N]^T$ and PS ratio vector $\boldsymbol{\rho} = [\rho_1, \ldots, \rho_N]^T$.

First we consider a simple scenario where there is only one user in the network. Given a target amount E_s of saved energy, we can obtain the boundary point (E_s, τ) of $\mathcal{C}_{E-T}$ by solving following convex optimization problem based on (3.4), (3.5) and (3.6)

$$\text{(P1)} \quad \underset{Q_1,\rho_1,B_1}{\text{maximize}} \quad \tau_1 = B_1 \tag{3.8a}$$

$$\text{s.t.} \quad B_1 \leq \frac{1}{2}\log_2(1 + \bar{\rho}_1 P\gamma_1) \tag{3.8b}$$

$$B_1 \leq \frac{1}{2}\log_2(1 + Q_1\gamma_d) \tag{3.8c}$$

$$E_s = \frac{1}{2}\eta\rho_1 P h_1 - \frac{1}{2}Q_1 \tag{3.8d}$$

$$Q_1 \geq 0, \quad 0 \leq \rho_1 \leq 1, \quad B_1 \geq 0 \tag{3.8e}$$

where $\bar{\rho}_1 = 1 - \rho_1$.

Lemma 3.3.1: The equality of (3.8b) and (3.8c) holds for the optimal solution of P2, denoted by ρ_1^*, Q_1^*.

Proof: Please refer to Appendix A. ■

According to *Lemma 3.3.1*, we derive the closed-form solutions of P1 as follows

$$Q_1^* = \frac{\gamma_1(\eta P h_1 - 2E_s)}{\gamma_1 + \eta\gamma_g h_1} = \beta Q_{\max} \tag{3.9a}$$

$$\rho_1^* = \frac{2E_s + Q_1^*}{\eta P h_1} \tag{3.9b}$$

$$B_1^* = \frac{1}{2}\log_2(1 + Q_1^*\gamma_g) \tag{3.9c}$$

where $\beta = \frac{\gamma_1}{\gamma_1 + \eta\gamma_g h_1}$ and $Q_{\max} = \eta P h_1 - 2E_s$, when $\rho_1 = 1$.

Fig. 3.3 is an example to illustrate the E-T tradeoff for the only one source S_1. We assume the distances from S_1 to R and from R to D are $d_1 = 1$ (unit) and $d_D = 1$. The path loss exponent is set to $\alpha = 2$, the average signal power attenuation at a reference of 1 unit of distance is set to $\lambda = 1$, and noise at R and D is set to -10 dBm (10^{-4}). Thus $\gamma_1 = 40$ dB. The transmission power by S_1 is $P = 200$ mW and the energy efficiency is $\eta = 0.75$. In Fig. 3.3a, we can see that when transmission power Q by the relay R is increasing, the amounts of data transmission achievable from S_1 to R, denoted by B_{sr}, is decreasing while the amounts of data transmission achievable from R to D, denoted by B_{rd} is increasing. With three different target amounts of saved energy $E_s = 10, 30, 60$ mJ, all the three trajectories of B_{sr} and B_{rd} meet at $Q_1^* = \beta Q_{\max}$, where the throughput of S_1 reaches maximum. By substituting our parameter settings into optimal solutions (3.9), $\beta = \frac{\gamma_1}{\gamma_1 + \eta\gamma_g h_1} = 0.57$ is obtained as shown in Fig. 3.3a. When the amount of saved energy E_s increases from 10 to 60 mJ, the maximum throughput τ^* decreases from 4.7 to 3.7. Moreover, the E-T tradeoff for S_1 is illustrated in Fig. 3.3b. It can be identified that when there is no energy left, the maximum throughput of S_1 is close to 5. The maximum amount of saved energy E_s is 75 mJ when data transmission is decreasing to zero for the one source scenario.

3.4 Throughput and Energy Tradeoffs in multi-source scenario

In this section, we consider two strategies in a multi-source network. One strategy is that all source nodes share a common PS ratio. The other is that each source node has an individual PS ratio. Based on different strategies, we formulate two convex optimization problems and illustrate the E-T tradeoffs between the amounts of saved energy and average throughputs for both two cases.

3.4.1 Common PS ratio

First, we consider a strategy where PS ratios for each source are equal at the relay. The common PS ratio is denoted by ρ_e, and the convex optimization problem for the boundary points (E_s, τ) of the E-T region is formulated as

$$\text{(P2)} \quad \underset{\boldsymbol{Q},\rho_e,\boldsymbol{B}}{\text{maximize}} \quad \tau = \frac{1}{N}\sum_{i=1}^{N} B_i \tag{3.10a}$$

$$\text{s.t.} \quad B_i \leq \frac{1}{2N}\log_2(1+\bar{\rho}_e P\gamma_i) \tag{3.10b}$$

$$B_i \leq \frac{1}{2N}\log_2(1+Q_i\gamma_d) \tag{3.10c}$$

$$E_s = \frac{1}{2N}\sum_{i=1}^{N}\eta\rho_e P h_i - \frac{1}{2N}\sum_{i=1}^{N} Q_i \tag{3.10d}$$

$$0 \leq \rho_e \leq 1 \tag{3.10e}$$

$$Q_i \geq 0, \quad B_i \geq 0 \tag{3.10f}$$

The enhanced *Newton Barrier* algorithm in Chapter 2.4 is adopted to solve this convex optimization problem.

Fig. 3.4 illustrates optimal transmission power Q_i^* and common PS ratio ρ_e^* under different target amount of saved energy E_s, and Fig. 3.5 shows the E-T tradeoffs for each source in the network. We assume that there are three source nodes in the network with distances from each source to R are $d_1 = 1, d_2 = 2$ and $d_3 = 3$, respectively. All the other parameters are the same to those in Section 3.3, so that $\gamma_1 = 40$ dB, $\gamma_2 = 34$ dB and $\gamma_3 = 20$ dB. From (3.10d), it is clear that the transmission power Q_i for each source and the common PS ratio ρ_e are linear to the saved energy E_s, which is observed in Fig. 3.4. Also from (3.10d), the maximum saved energy can be derived as $E_{\max} = \frac{1}{2N}\sum_{i=1}^{N}\eta P h_i = 34$

mJ, when $\rho_e = 1$ and $Q_i = 0$ with $i = 1, 2, 3$, as shown in Fig 3.4 and 3.5. From Fig. 3.4(a), S_1 with the best channel condition is allocated with the largest transmission power, hence we see that S_1 has the largest throughput in Fig. 3.5. This is in agreement with the intuition that the source with the best channel condition is supposed to make the most contribution to the average performance of the network.

3.4.2 Individual Optimal PS Ratios

In this part, we consider a strategy where each source has an individual PS ratio ρ_i at the relay R. In such scenario, the convex optimization problem is formulated as

$$\text{(P3)} \quad \underset{\boldsymbol{Q},\boldsymbol{\rho},\boldsymbol{B}}{\text{maximize}} \quad \tau = \frac{1}{N}\sum_{i=1}^{N} B_i \tag{3.11a}$$

$$\text{s.t.} \quad E = \frac{1}{2N}\sum_{i=1}^{N} \eta\rho_i P h_i - \frac{1}{2N}\sum_{i=1}^{N} Q_i \tag{3.11b}$$

$$B_i \leq \frac{1}{2N}\log_2(1 + \bar{\rho}_i P\gamma_i) \tag{3.11c}$$

$$B_i \leq \frac{1}{2N}\log_2(1 + Q_i\gamma_d) \tag{3.11d}$$

$$Q_i \geq 0, \quad 0 \leq \rho_i \leq 1 \tag{3.11e}$$

where $\bar{\rho}_i = 1 - \rho_i$.

Using the same parameter settings in the previous part, E-T tradeoffs for each user source with individual optimal PS ratios are illustrated in Fig. 3.6. In Fig. 3.6(a), it can be observed that optimal ρ_1 for S_1 with the best channel conditions is always larger than ρ_2 and ρ_3. Moreover, it is interesting to find that there is a particular value for E_s, denoted by E_t, e.g., $E_t \approx 15$ in Fig. 3.6. Specifically, in Fig. 3.6(a), inclination angles of three trajectories for PS ratios when $E_s < E_t$ are different from $E_s > E_t$. And in Fig. 3.6(b), all three sources have same throughputs from $E_s = E_t$ until E_s reaches the maximum value $E_{\max} = 34$ mJ.

3.5 Numerical Results

In the numerical study reported below, all receiver noise was set to 10^{-4}, and the energy conversion efficiency was set to $\eta = 0.75$. There were three source nodes in the network, and the distance from each source S_i to the relay R were set as $d_1 = 1, d_2 = 2$ and $d_3 = 3$,

respectively.

3.5.1 Performances versus path loss exponent α

In this part of the simulations, the transmission power of sources was fixed to P = 200 mW and performances of the network with different path loss exponent α were investigated. In Fig. 3.7, if all sources share the same PS ratio ρ_e, the optimal common PS ratios versus the amount of saved energy E_s are illustrated when the path loss exponent α =2, 2.5 and 3, respectively. We see that all three trajectories of ρ_e meet at the same point (E_{s0}, ρ_{e0}). When $E_s < E_{s0}$, the optimal ρ_e with lower path loss exponent α is greater than that with larger α. However, when $E_s > E_{s0}$, the optimal ρ_e with larger α is greater than that with lower α.

Next, comparisons of E-T tradeoffs with the common PS ratio and with individual PS ratios with different path loss exponent α are illustrated in Fig. 3.8. Intuitively, the larger path loss exponent α leads to poorer channel condition and thus worse average throughput, which is proved in Fig. 3.8. It is also observed that the average throughput with the individual PS ratios outperforms that with the common PS ratio, which is expected in our analysis.

3.5.2 Performances versus transmission power P of sources

In this part of the simulations, the path loss exponent was fixed to $\alpha = 2$ and performances of the network with different transmission power P were investigated. The optimal common PS ratio ρ_e versus the amount of saved energy E_s under different transmission power P is shown in Fig. 3.9. We observe that the increasing speed of the common PS ratio ρ_e gets smaller when the transmission power of sources P increases from 100 mW to 300 mW. This indicates that the relay will raise the ID ratio when the transmission power of received signals increases.

On the other hand, Fig. 3.10 compares T-E tradeoffs from the common PS ratio strategy with the individual PS ratio strategy under different transmission power P. First, it is in agreement with Fig. 3.8 that individual PS ratio strategy outperforms the common PS ratio strategy. And it can be also observed that the larger transmission power P is more beneficial to both strategies. Furthermore, when E_s increases, the fading speed of the average throughput with $P = 100$ mW is much larger than that with $P = 200$ mW and $P = 300$ mW. This indicates that the network with lower transmission power P is more sensitive to the changes of other system parameters, e.g., changes of target saved energy E_s.

3.6 Summary

In this chapter, we proposed a new cooperative wireless communication network protocol with multiple sources and one relay. *Energy-Throughput* (E-T) tradeoff regions are characterized between the maximum achievable average throughput of the sources and the total amount of saved energy in three circumstances. When there is only one source node, the closed-form solution is derived by solving KKT conditions. When there are multiple source nodes, we consider two strategies: one is common power splitting (PS) ratio strategy that the relay adopts the same PS ratio for all sources; the other is individual PS ratio strategy that each source uses an individual optimal PS ratio. Optimal solutions to the proposed convex optimization problems are obtained via the Newton Barrier algorithm developed in Chapter 2. Numerical results have shown that individual PS ratio strategy outperforms than the common PS ratio strategy.

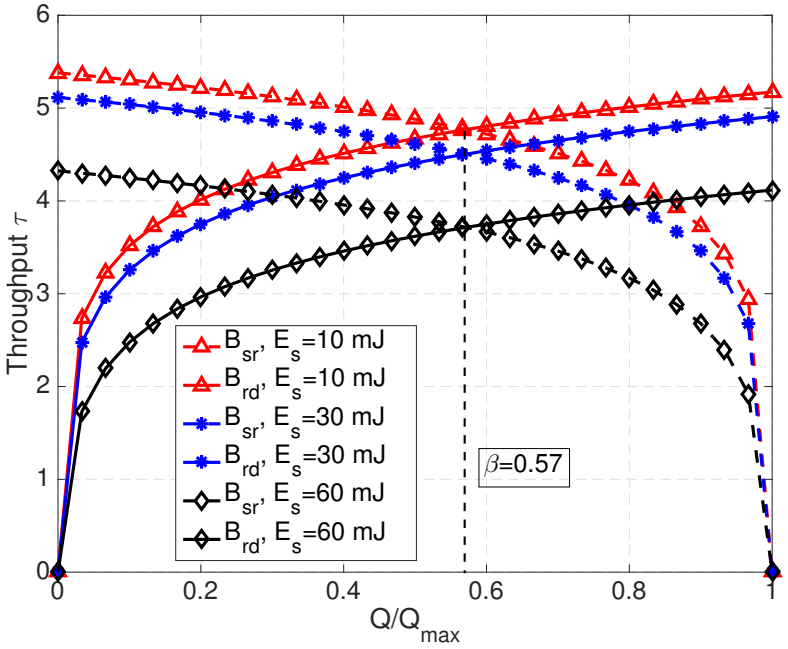

(a) τ versus Q_1

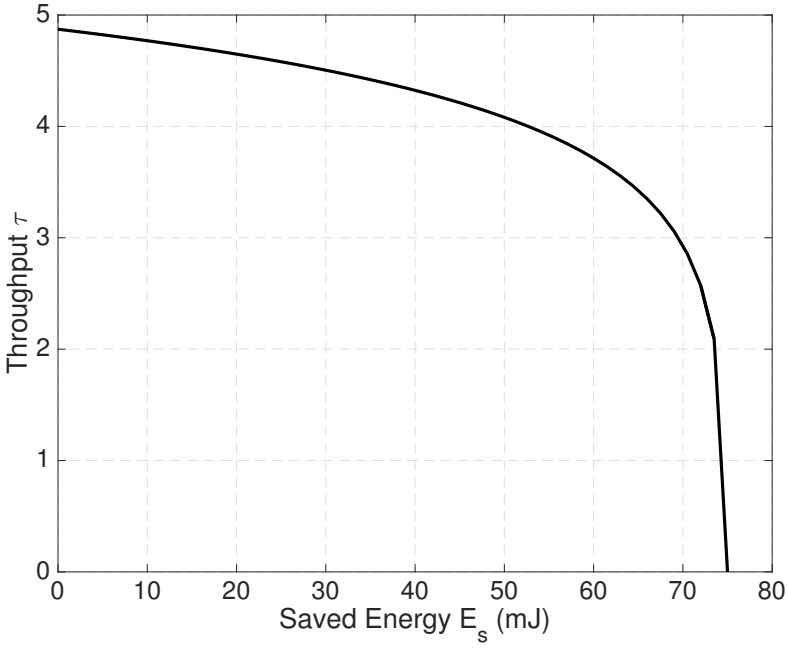

(b) τ versus E_s

Figure 3.3: (a) Throughput maximization (dashed lines are B_{sr}, solid lines are B_{rd}) versus transmission power by the single source S_1 and (b) E-T tradeoff for S_1.

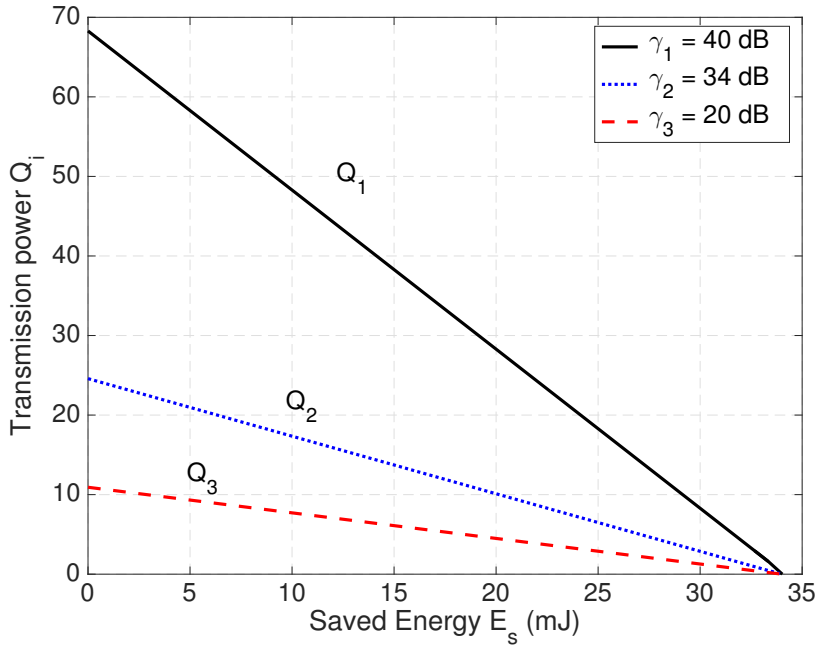

(a) optimal Q_i versus E_s

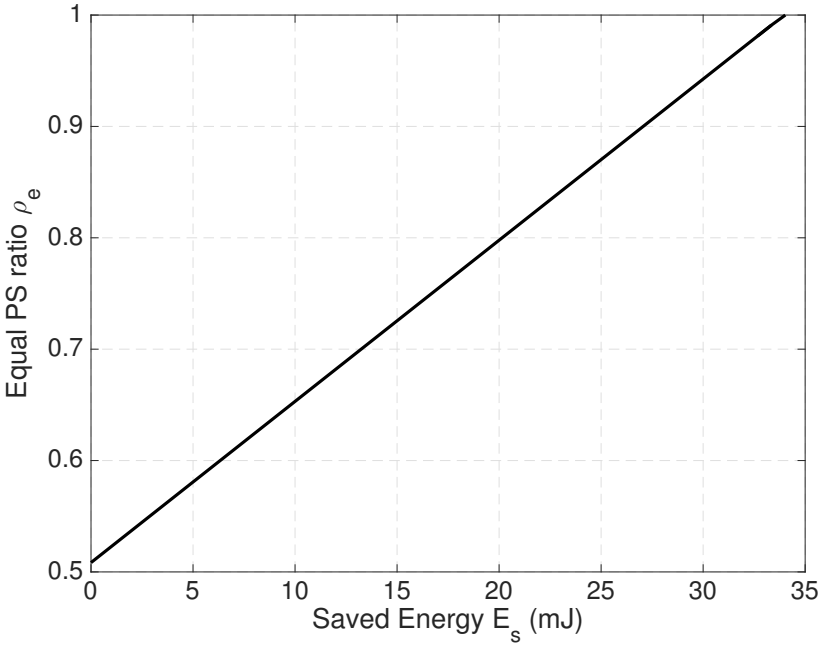

(b) optimal ρ_e versus E_s

Figure 3.4: (a) Optimal transmission power versus saved energy amount and (b) optimal common PS ratio ρ_e versus saved energy amount in a multi-source network.

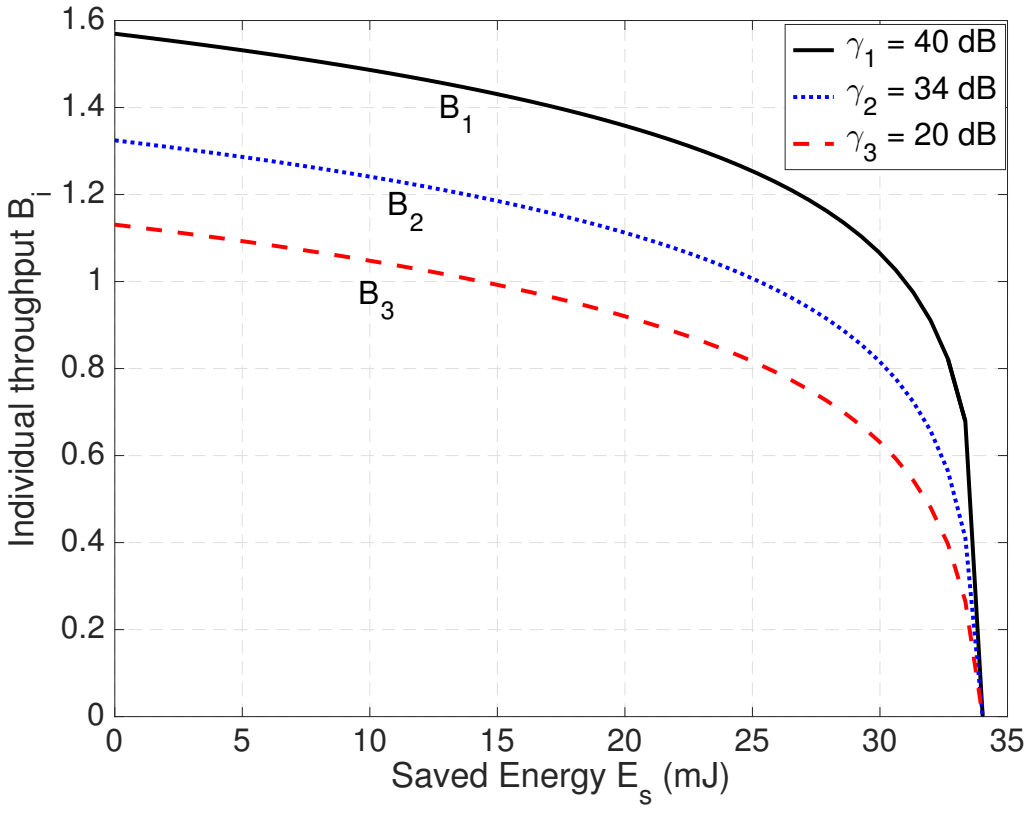

Figure 3.5: E-T tradeoffs for each user source with equal PS ratios in a multi-source network.

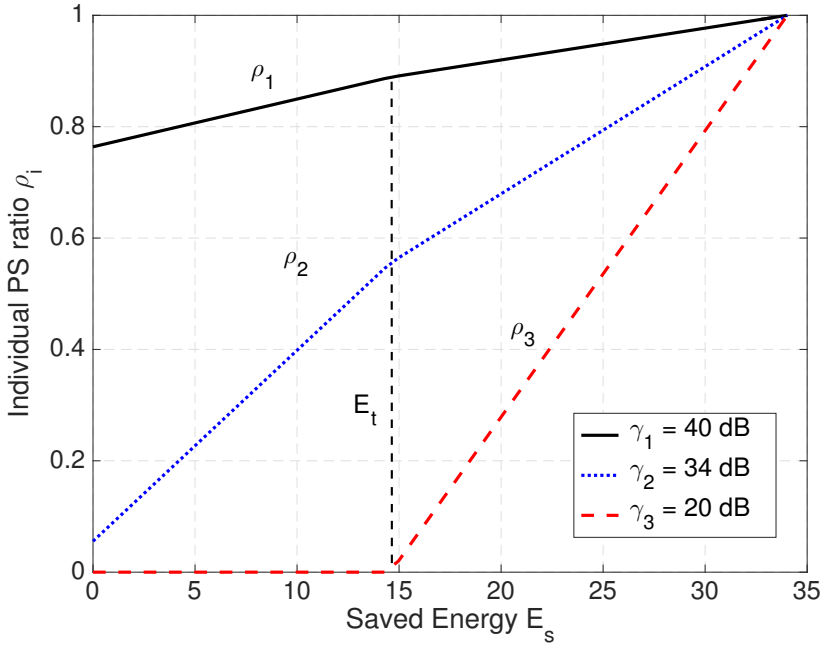

(a) optimal ρ_i versus E_s

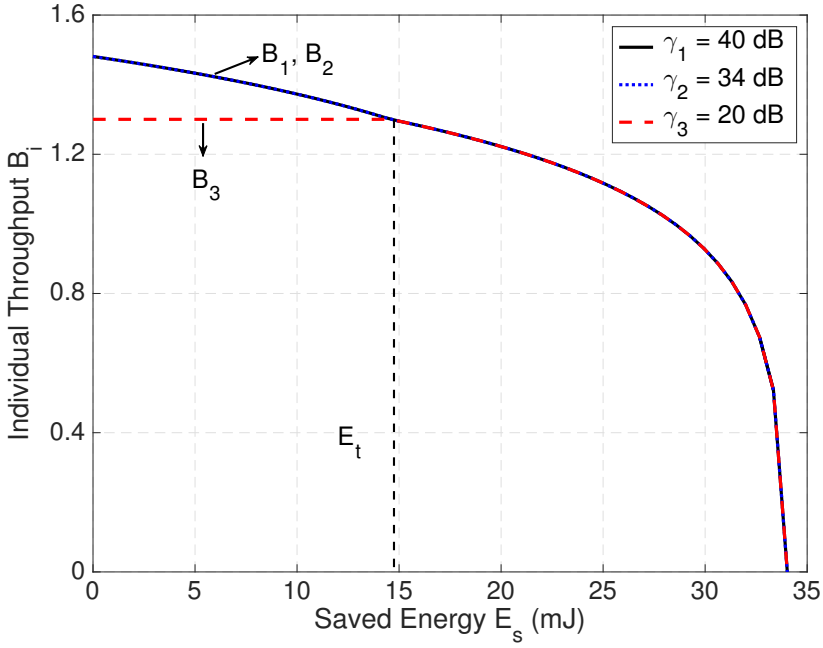

(b) maximum B_i versus E_s

Figure 3.6: (a) Optimal individual PS ratios versus the amounts of saved energy and (b) E-T tradeoffs for each user source with individual optimal PS ratios in a multi-source network.

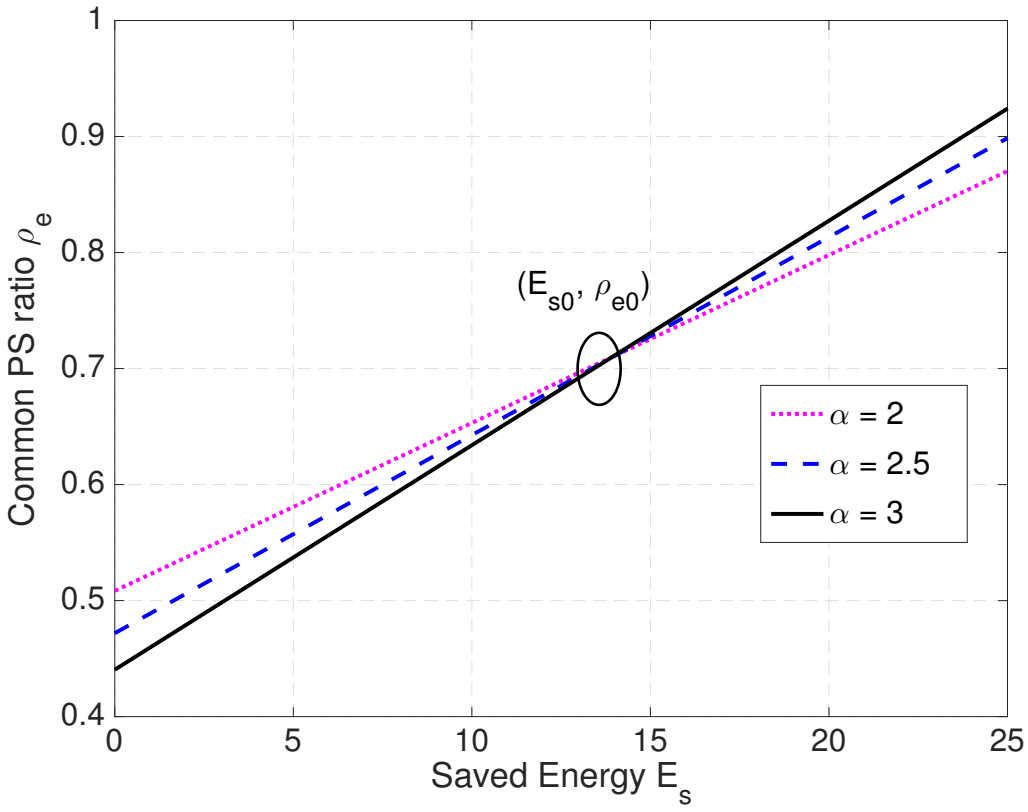

Figure 3.7: Common PS ratios ρ_e with different path loss exponent α in a three-source network.

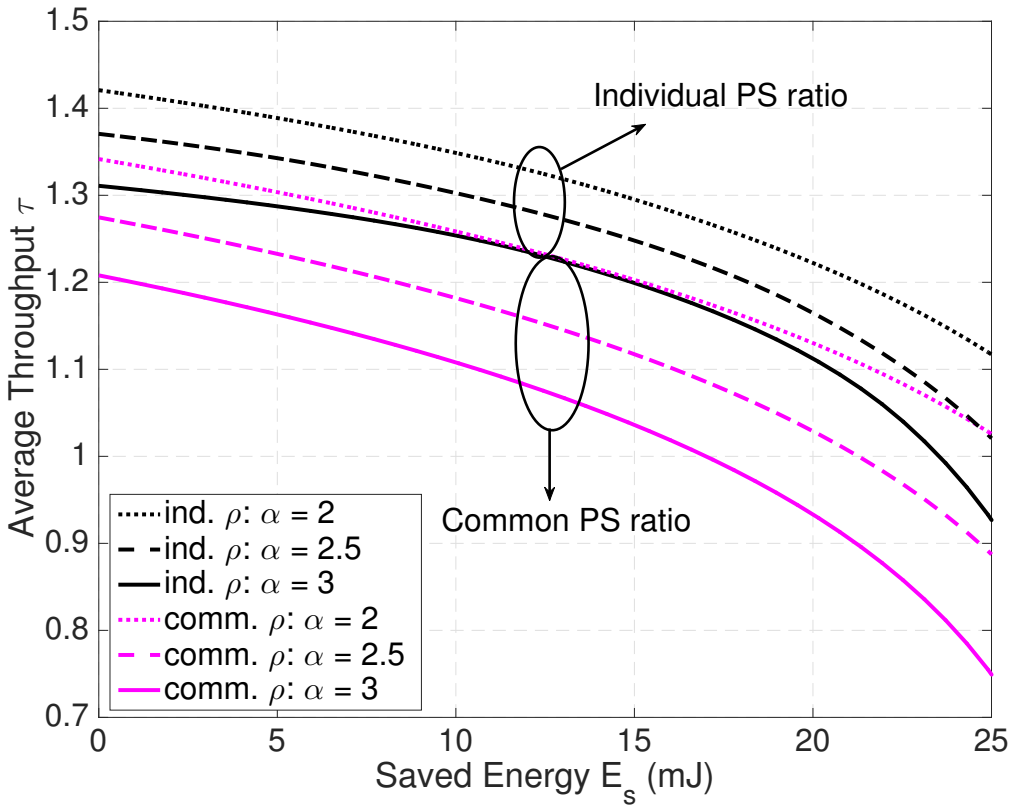

Figure 3.8: Comparisons of E-T tradeoffs in individual PS ratio case and common PS ratio case with different path loss exponent α in a three-source network.

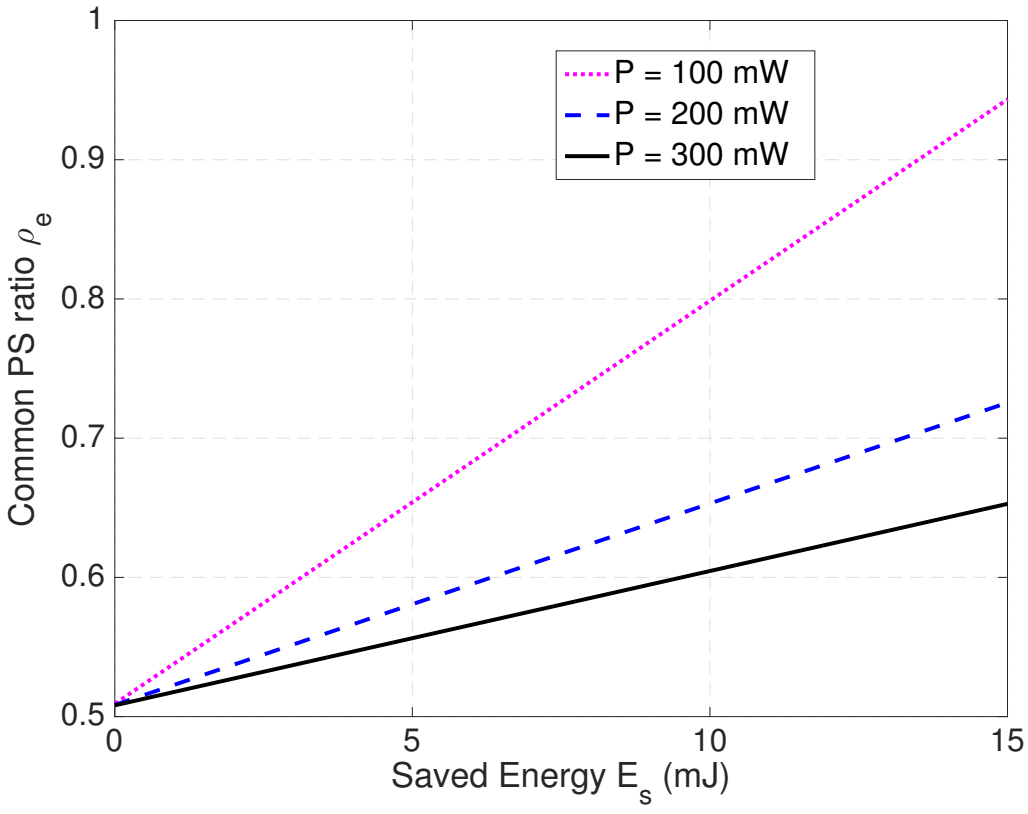

Figure 3.9: Common PS ratios ρ_e with different transmission power of sources P in a three-source network.

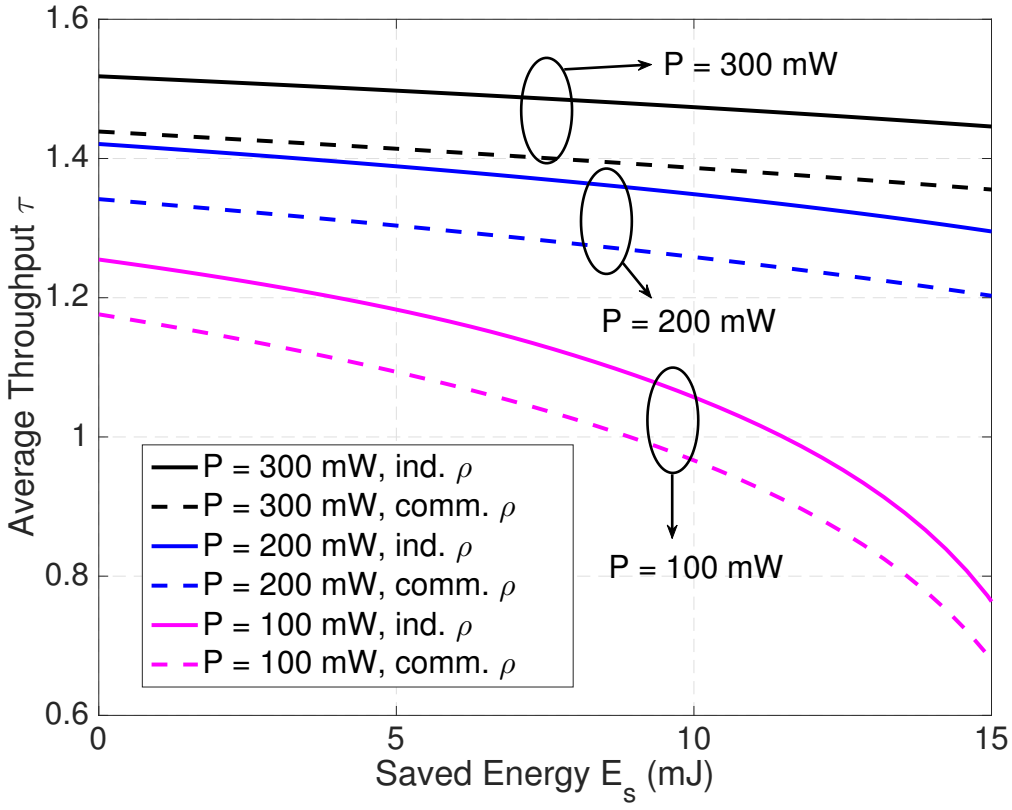

Figure 3.10: Comparisons of E-T tradeoffs in individual PS ratio case and common PS ratio case with different transmission power of sources P in a three-source network.

Chapter 4

Conclusion and future work

This thesis studies two wireless EH communication systems with joint energy cooperation and data cooperation. Chapter 2 considers a three-node model with two EH user nodes and a destination node, while Chapter 3 investigates a multi-source network with one EH relay but multiple sources. This chapter concludes the above research topics and presents some open issues and expectations for the future research.

4.1 Optimal Energy Management Strategies in Wireless Communications with Joint Data and Energy Cooperation

In this thesis, we have proposed an adaptive cooperative wireless communication network strategy that incorporates energy cooperation (EC) and data cooperation (DC). By examining a three-node network for detailed analysis under the proposal, optimal energy management strategies in terms of maximal weighted sum-throughput or minimum throughput of the two users are investigated in detail for four possible scenarios. Numerical results have shown that whether to include EC and DC depends on the availability of natural energy for harvesting and the topology of the nodes, and that employing EC strategies is of help when disparity between energy arrival rates of two users exists. We also observe that when two user nodes are sufficiently close, both EC and DC strategies are shown to be more effective.

4.2 Optimal Energy Management Strategies in Wireless Energy Harvesting Communications with Multiple Sources

In this thesis, we also proposed a new cooperative wireless communication network protocol with multiple sources and one relay. When there is only one source node, the closed-form solution is derived by solving KKT conditions. When there are multiple source nodes, we propose two strategies: one is common PS ratio strategy that the relay adopts the same PS ratio for all sources; the other is individual PS ratio strategy that each source uses an individual optimal PS ratio for the overall performance. The Energy-Throughput (E-T) tradeoffs are investigated in detail for above three cases. Numerical results have shown that individual PS ratio strategy outperforms than the common PS ratio strategy, and the network with higher transmission power by sources are more adaptive to the changes of other system parameters.

4.3 Future Work

There are several issues appear to be worthwhile for future research. These include:

- As an initial study of optimal energy strategies with joint energy cooperation and data cooperation, in this thesis we have focused on problem formulation and algorithm development. The channel model and energy arrival conditions are relatively simple. More realistic channel models with increased degree of complexity should be investigated in the future.

- This thesis considers only one transmission block where the energy harvested is exhausted for information transmission. In practice, the system performance can be improved if user nodes can accumulate the energy and perform energy scheduling across multiple consecutive blocks.

- Currently only limited number of user nodes are considered in our model. It would be of interest to extend the proposed scheme to large scale cooperative networks in the future research.

Appendix A

A proof of Lemma 3.3.1

From (3.8d), we can derive the optimal PS ratio $\rho_1^* = \frac{2E_s+Q_1^*}{\eta P h_1}$ and eliminate the PS ratio variable by doing such substitution as follows

$$\begin{aligned}
\underset{Q_1,B_1}{\text{maximize}} \quad & B_1 && \text{(A.1a)}\\
\text{s.t.} \quad & B_1 \leq \frac{1}{2}\log_2(1+(1-\frac{2E_s+Q_1}{\eta P h_1})P\gamma_1) && \text{(A.1b)}\\
& B_1 \leq \frac{1}{2}\log_2(1+Q_1\gamma_d) && \text{(A.1c)}\\
& Q_1 \geq 0 && \text{(A.1d)}\\
& \frac{2E_s+Q_1}{\eta P h_1} \leq 1 && \text{(A.1e)}
\end{aligned}$$

The Lagrangian of convex problem (A.1) is given by

$$\begin{aligned}
\mathcal{L}_1(B_1,Q_1,\boldsymbol{\mu}) = & -B_1 + \mu_1(B_1 - \frac{1}{2}\log_2(1+(1-\frac{2E_s+Q_1}{\eta P h_1})P\gamma_1))\\
& + \mu_2(B_1 - \frac{1}{2}\log_2(1+Q_1\gamma_d)) - \mu_3 Q_1 + \mu_4(\frac{2E_s+Q_1}{\eta P h_1} - 1)
\end{aligned} \tag{A.2}$$

The Karush-Kuhn-Tucker (KKT) conditions for optimal solutions $(Q_1^*, \boldsymbol{\mu}^*)$ are expressed as

$$\frac{\partial \mathcal{L}_1}{\partial B_1^*} = -1 + \mu_1^* + \mu_2^* = 0 \tag{A.3a}$$

$$\frac{\partial \mathcal{L}_1}{\partial Q_1^*} = \frac{\mu_1^*}{2} \frac{\frac{\gamma_1}{\eta h_1}}{(1 + (1 - \frac{2E_s + Q_1^*}{\eta P h_1}) P\gamma_1) \ln 2} - \frac{\mu_2^*}{2} \frac{\gamma_d}{(1 + Q_1^* \gamma_d) \ln 2} - \mu_3^* + \frac{\mu_4^*}{\eta P h_1} = 0 \tag{A.3b}$$

$$\mu_1^* (B_1^* - \frac{1}{2} \log_2(1 + (1 - \frac{2E_s + Q_1^*}{\eta P h_1}) P\gamma_1)) = 0 \tag{A.3c}$$

$$\mu_2^* (B_1^* - \frac{1}{2} \log_2(1 + Q_1^* \gamma_d)) = 0 \tag{A.3d}$$

$$\mu_3^* Q_1^* = 0 \tag{A.3e}$$

$$\mu_4^* (\frac{2E_s + Q_1^*}{\eta P h_1} - 1) = 0 \tag{A.3f}$$

$$\mu_i^* \geq 0, \quad i = 1, 2, 3, 4 \tag{A.3g}$$

$$Q_1^* \geq 0 \tag{A.3h}$$

1) If $\frac{2E_s + Q_1^*}{\eta P h_1} = 1$ or $Q_1^* = 0$, throughput of S_1 is zero, i.e., $B_i^* = 0$, which is a meaningless case that we do not take into account in practice.

2) If $\frac{2E_s + Q_1^*}{\eta P h_1} < 1$ and $Q_1^* > 0$, we have $\mu_3^* = 0$ and $\mu_4^* = 0$ based on (A.3e) and (A.3f). By solving (A.3a) and (A.3b), we derive the optimal Lagrangian multipliers as follows

$$\mu_1^* = \frac{z_1^*}{1 + z_1^*} \tag{A.4a}$$

$$\mu_2^* = \frac{1}{1 + z_1^*} \tag{A.4b}$$

where $z_1^* = \frac{r_d}{1 + Q_1^* r_d} (\frac{\eta h_1}{\gamma_1} + \eta h_1 P - 2E_s - Q_1^*)$. Because both μ_1^* and μ_2^* are positive, the equality of (3.8b) and (3.8c) holds. This completes the proof of *Lemma 1*.

Appendix B

Key MATLAB functions for Newton Barrier algorithm

Below is Newton Barrier function to find an optimal solution xs:

```
% Use Newton Barrier to solve problem P1-A.
% Output: optimal solution xs
% xs(1) = B; xs(2) = t1; xs(3) = t2; xs(4) = t3; xs(5) = t4;
   xs(6) = t5; xs(7) = y1; xs(8) = y2; xs(9) = y3; xs(10) = y4;
   xs(11) = y5;
% Input:
% x0: a feasible initializiation of soltuion
% A,b: linear conditions, where A*x <= b
% gam: array of SNRs
% epsi: tolerance
function [xs,fs,k] = newton(x0,epsi,A,b,gam)
k = 1;
xk = x0;
gk = gradient(xk,gam);
hk = hessian(xk,gam);
dk = -inv(hk)*gk;
dhk = A*dk;
bw = b - A*xk;
if(dhk < 0)
  a_tmp1 = 1;
else
```

```
  ind = find(dhk > 0);
  a_tmp1 = 0.99*min(bw(ind)./dhk(ind));
end
ak = golden_sect('afunc',a_max,xk,dk,gam);
adk = ak*dk;
er = norm(adk);
while (er > epsi),
  xk = xk + adk;
  gk = gradient(xk,gam);
  hk = hessian(xk,gam);
  dk = -inv(hk)*gk;
  dhk = A*dk;
  bw = b - A*xk;
  if(dhk < 0)
    a_tmp1 = 1;
  else
    ind = find(dhk > 0);
    a_tmp1 = 0.99*min(bw(ind)./dhk(ind));
  end
  ak = golden_sect('afunc',a_max,xk,dk,gam);
  adk = ak*dk;
  er = norm(adk);
end
% Solution point
xs = xk + adk;
% Objective function at the solution point
fs = fun0(xs,gam);
```

Below is Golden-Section Search function to find a optimal step size a:

```
function [a] = golden_sect(fname,xL1,xU1,rou,xk,dk,p)
% Generate xa1, xb1, f(xa1), and f(xb1)
K = 0.5*(1+sqrt(5));
k = 1;
I1 = xU1 - xL1;
I2 = I1/K;
xak = xU1 - I2;
xbk = xL1 + I2;
```

```
fak = feval(fname,xak,xk,dk,p);
fbk = feval(fname,xbk,xk,dk,p);
Ik1 = I2;
xLk = xL1;
xUk = xU1;
xw = xak;
% Perform Golden-Section search
while Ik1 >= rou & xak <= xbk,
  Ik2 = Ik1/K;
  if fak >= fbk,
    xLk1 = xak;
    xUk1 = xUk;
    xak1 = xbk;
    xbk1 = xLk1 + Ik2;
    fak1 = fbk;
    fbk1 = feval(fname,xbk1,xk,dk,p);
    xw = 0.5*(xak1 + xUk1);
  else
    xLk1 = xLk;
    xUk1 = xbk;
    xak1 = xUk1 - Ik2;
    xbk1 = xak;
    fbk1 = fak;
    fak1 = feval(fname,xak1,xk,dk,p);
    xw = 0.5*(xLk1 + xbk1);
  end
  xLk = xLk1;
  xUk = xUk1;
  xak = xak1;
  xbk = xbk1;
  fak = fak1;
  fbk = fbk1;
  Ik1 = Ik2;
  k = k + 1;
end
a = xw;
```

Appendix C

Key MATLAB function for local quadratic approximation algorithm

```
% To solve QCQP problem for problem P1-A.
% Output: optimal solution xs
% xs(1) = B; xs(2) = t1; xs(3) = t2; xs(4) = t3; xs(5) = t4;
   xs(6) = t5; xs(7) = y1; xs(8) = y2; xs(9) = y3; xs(10) = y4;
   xs(11) = y5;
% input:
% x0: a feasible initializiation of soltuion
% A,b: linear conditions, where A*x <= b
% gam: array of SNRs
% epsi1, epsi2: tolerance
function [xs,fs,iter] = qcqp_p1a(x0,A,b,gam,epsi1,epsi2)
n1 = 11; % number of design variables
n2 = 18; % number of constraints
muk = mu0;
iter = 0;
x0w = x0;
err2 = 1;
while err2 >= epsi2,
% generate gradients and hessians of objective funtion and
   non-linear constraints
  [g0,v0,c1,g1,v1,c2,g2,v2] = gen_data(x0w);
  H0 = v0*v0';
```

```
H1 = v1*v1';
H2 = v2*v2';
xk = x0w;
dk = d0;
f0 = func0(xk,gam,w1,w2);
fk_old = f0;
% mu1, mu2: lagrange multipliers for two non-linear constraints
mu1 = muk(1);
mu2 = muk(2);
% mu3: lagrange multipliers for linear constraints
mu3 = muk(3:n2);
bw = b - A*xk;
qk = bw - A*dk;;
qki = 1./qk;
d = min(1e+16,mu3.*qki);
Ad = diag(d)*A;
h0 = H0*dk + g0;
h1 = H1*dk + g1;
h2 = H2*dk + g2;
rd1 = -(0.5*(norm(v1'*dk))^2 + g1'*dk + c1);
rd2 = -(0.5*(v2'*dk)^2 + g2'*dk + c2);
rp = -(h0 + mu1*h1 + mu2*h2 + A'*mu3);
gap = mu1*rd1 + mu2*rd2 + mu3'*qk;
tau = gap/rho_q;
k = 0;
err1 = 1;
while err1 >= epsi1,
  % Calculate d_x and d_mu
  H = H0 + mu1*H1 + mu2*H2 + (mu1/rd1)*(h1*h1') +
      (mu2/rd2)*(h2*h2') + A'*Ad;
  rpt = rp + (mu1-tau/rd1)*h1 + (mu2-tau/rd2)*h2 +
     A'*(mu3-tau*qki);
  d_x = H\rpt;
  d_mu1 = (mu1/rd1)*(h1'*d_x) + tau/rd1 - mu1;
  d_mu2 = (mu2/rd2)*(h2'*d_x) + tau/rd2 - mu2;
  d_mu3 = Ad*d_x + tau*qki - mu3;
  % Calculate step size
```

```
dhk = A*d_x;
if(dhk < 0)
  a1 = 1;
else
  ind = find(dhk > 0);
  a1 = min(qk(ind)./dhk(ind));
end
t10 = 0.5*(norm(v1'*d_x)^2);
t11 = h1'*d_x;
t12 = c1 + 0.5*(norm(v1'*dk)^2) + g1'*dk;
a21 = real((sqrt(t11^2-4*t10*t12) - t11)/(2*t10));
t20 = 0.5*(v2'*d_x)^2;
t21 = h2'*d_x;
t22 = c2 + 0.5*(v2'*dk)^2 + g2'*dk;
a22 = real((sqrt(t21^2-4*t20*t22) - t21)/(2*t20));
ax = 0.99*min([a1 a21 a22]);
ax = max([ax 1e-6]);
if d_mu1 >= 0,
  au1 = 1;
else
  au1 = -mu1/d_mu1;
end
if d_mu2 >= 0,
  au2 = 1;
else
  au2 = -mu2/d_mu2;
end
ind = find(d_mu3 < 0);
au3 = min(-mu3(ind)./d_mu3(ind));
au = 0.99*min([au1 au2 au3]);
a0 = -(h0'*d_x)/(v0'*d_x)^2;
a01 = -(H0*d_x)\h0;
if a0 > 0,
  a = min([a0 ax]);
else
  a = 1e-5*ax;
end
```

```
  % Generate a new iterate
  dk = dk + a*d_x;
  mu1 = mu1 + au*d_mu1;
  mu2 = mu2 + au*d_mu2;
  mu3 = mu3 + au*d_mu3;
  qk = bw - A*dk;
  qki = 1./qk;
  h0 = H0*dk + g0;
  h1 = H1*dk + g1;
  h2 = H2*dk + g2;
  rd1 = -(0.5*(norm(v1'*dk))^2 + g1'*dk + c1);
  rd2 = -(0.5*(v2'*dk)^2 + g2'*dk + c2);
  gap = mu1*rd1 + mu2*rd2 + mu3'*qk;
  tau = gap/rho_q;
  rp = -(h0 + mu1*h1 + mu2*h2 + A'*mu3);
  fk = func0(xk+dk,gam1,w1,w2);
  err1 = abs((fk_old-fk)/fk);
  fk_old = fk;
  k = k + 1;
end
% update xk and muk
xk = xk + dk;
muk_new = [mu1; mu2; mu3];
dm = muk_new - muk;
muk = muk_new;
x0w = xk;
iter = iter + 1;
%k
err2 = 1/(sqrt(n1)+sqrt(n2))*(norm(dk)+norm(dm));
end
xs = xk;
```

Bibliography

[1] S. Bi, C. K. Ho, and R. Zhang, "Wireless powered communication: Opportunities and challenges," *IEEE Communications Magazine*, vol. 53, no. 4, pp. 117–125, 2015.

[2] I. Krikidis, S. Timotheou, S. Nikolaou, G. Zheng, D. W. K. Ng, and R. Schober, "Simultaneous wireless information and power transfer in modern communication systems," *IEEE Communications Magazine*, vol. 52, no. 11, pp. 104–110, Nov. 2014.

[3] S. Bi and R. Zhang, "Placement optimization of energy and information access points in wireless powered communication networks," *IEEE transactions on wireless communications*, vol. 15, no. 3, pp. 2351–2364, Mar. 2016.

[4] O. Orhan and E. Erkip, "Energy harvesting two-hop communication networks," *IEEE Journal on Selected Areas in Communications*, vol. 33, no. 12, pp. 2658–2670, Dec. 2015.

[5] S. Sudevalayam and P. Kulkarni, "Energy harvesting sensor nodes: Survey and implications," *IEEE Communications Surveys & Tutorials*, vol. 13, no. 3, pp. 443–461, 2011.

[6] X. Jiang, J. Polastre, and D. Culler, "Perpetual environmentally powered sensor networks," in *Proc. 4th International Symposium on Information Processing in Sensor Networks (IPSN'05)*, Apr. 2005.

[7] K. Tutuncuoglu and A. Yener, "Optimum transmission policies for battery limited energy harvesting nodes," *IEEE Transactions on Wireless Communications*, vol. 11, no. 3, pp. 1180–1189, 2012.

[8] M. Gregori and M. Payaró, "Energy-efficient transmission for wireless energy harvesting nodes," *IEEE Transactions on Wireless Communications*, vol. 12, no. 3, pp. 1244–1254, 2013.

[9] O. Orhan, D. Gunduz, and E. Erkip, "Throughput maximization for an energy harvesting communication system with processing cost," in *Information Theory Workshop (ITW), 2012 IEEE*. IEEE, 2012, pp. 84–88.

[10] J. Yang and S. Ulukus, "Optimal packet scheduling in an energy harvesting communication system," *IEEE Transactions on Communications*, vol. 60, no. 1, pp. 220–230, Jan. 2012.

[11] S. Luo, R. Zhang, and T. J. Lim, "Optimal save-then-transmit protocol for energy harvesting wireless transmitters," *IEEE Transactions on Wireless Communications*, vol. 12, no. 3, pp. 1196–1207, Mar. 2013.

[12] W. C. Brown, "The history of power transmission by radio waves," *IEEE Transactions on Microwave Theory and Techniques*, vol. 32, no. 9, pp. 1230–1242, Sep. 1984.

[13] X. Lu, P. Wang, D. Niyato, D. I. Kim, and Z. Han, "Wireless networks with RF energy harvesting: A contemporary survey," *IEEE Communications Surveys & Tutorials*, vol. 17, no. 2, pp. 757–789, 2015.

[14] H. Nishimoto, Y. Kawahara, and T. Asami, "Prototype implementation of ambient rf energy harvesting wireless sensor networks," in *Proceedings of IEEE Sensors*. IEEE, Nov. 2010, pp. 1282–1287.

[15] L. R. Varshney, "Transporting information and energy simultaneously," in *IEEE International Symposium on Information Theory (ISIT)*, Jul. 2008, pp. 1612–1616.

[16] R. Zhang and C. K. Ho, "MIMO broadcasting for simultaneous wireless information and power transfer," *IEEE Transactions on Wireless Communications*, vol. 12, no. 5, pp. 1989–2001, Mar. 2013.

[17] L. Liu, R. Zhang, and K.-C. Chua, "Wireless information transfer with opportunistic energy harvesting," *IEEE Transactions on Wireless Communications*, vol. 12, no. 1, pp. 288–300, 2013.

[18] H. Tabassum, E. Hossain, A. Ogundipe, and D. I. Kim, "Wireless-powered cellular networks: Key challenges and solution techniques," *IEEE Communications Magazine*, vol. 53, no. 6, pp. 63–71, Jun. 2015.

[19] S. Bi, Y. Zeng, and R. Zhang, "Wireless powered communication networks: An overview," *IEEE Wireless Communications*, vol. 23, no. 2, pp. 10–18, May 2016.

[20] B. Gurakan, O. Ozel, J. Yang, and S. Ulukus, "Energy cooperation in energy harvesting wireless communications," in *IEEE International Symposium on Information Theory (ISIT)*, Jul. 2012, pp. 965–969.

[21] B. Gurakan, O. Ozel, J. Yang, and S. Ulukus, "Two-way and multiple-access energy harvesting systems with energy cooperation," in *the Forty Sixth Asilomar Conference on Signals, Systems and Computers (ASILOMAR)*. IEEE, Nov. 2012, pp. 58–62.

[22] X. Huang and N. Ansari, "Energy sharing within EH-enabled wireless communication networks," *IEEE Wireless Communications*, vol. 22, no. 3, pp. 144–149, Jun. 2015.

[23] K. Tutuncuoglu and A. Yener, "Cooperative energy harvesting communications with relaying and energy sharing," in *Information Theory Workshop (ITW)*. IEEE, Sep. 2013, pp. 1–5.

[24] N. Su, O. Kaya, S. Ulukus, and M. Koca, "Cooperative multiple access under energy harvesting constraints," in *Global Communications Conference (GLOBECOM)*. IEEE, Dec. 2015, pp. 1–6.

[25] W. Ni and X. Dong, "Energy harvesting wireless communications with energy cooperation between transmitter and receiver," *IEEE Transactions on Communications*, vol. 63, no. 4, pp. 1457–1469, Apr. 2015.

[26] F. Benkhelifa and M.-S. Alouini, "Simultaneous wireless information and power transfer for mimo amplify-and-forward relay systems," in *Global Communications Conference (GLOBECOM), 2015 IEEE*. IEEE, Dec. 2015, pp. 1–6.

[27] Z. Ding and H. V. Poor, "Cooperative energy harvesting networks with spatially random users," *IEEE Signal Processing Letters*, vol. 20, no. 12, pp. 1211–1214, Dec. 2013.

[28] I. Krikidis, S. Sasaki, S. Timotheou, and Z. Ding, "A low complexity antenna switching for joint wireless information and energy transfer in mimo relay channels," *IEEE Transactions on Communications*, vol. 62, no. 5, pp. 1577–1587, May 2014.

[29] Z. Chen, B. Xia, and H. Liu, "Wireless information and power transfer in two-way amplify-and-forward relaying channels," in *IEEE Global Conference on Signal and Information Processing (GlobalSIP)*. IEEE, Dec 2014, pp. 168–172.

[30] I. Krikidis, "Simultaneous information and energy transfer in large-scale networks with/without relaying," *IEEE Transactions on Communications*, vol. 62, no. 3, pp. 900–912, Mar. 2014.

[31] B. K. Chalise, W.-K. Ma, Y. D. Zhang, H. A. Suraweera, and M. G. Amin, "Optimum performance boundaries of OSTBC based AF-MIMO relay system with energy harvesting receiver," *IEEE Transactions on Signal Processing*, vol. 61, no. 17, pp. 4199–4213, Sep. 2013.

[32] R. Allan, "Energy harvesting powers wireless sensor networks in industrial apps," Available: http://www.electronicdesign.com/4g/energy-harvesting-powers-wireless-sensor-networks-industrial-apps, Sep. 2012.

[33] O. Ozel, K. Tutuncuoglu, J. Yang, S. Ulukus, and A. Yener, "Transmission with energy harvesting nodes in fading wireless channels: Optimal policies," *IEEE Journal on Selected Areas in Communications*, vol. 29, no. 8, pp. 1732–1743, Sep. 2011.

[34] C. K. Ho and R. Zhang, "Optimal energy allocation for wireless communications with energy harvesting constraints," *IEEE Transactions on Signal Processing*, vol. 60, no. 9, pp. 4808–4818, Sep. 2012.

[35] L. Liu, R. Zhang, and K.-C. Chua, "Wireless information and power transfer: A dynamic power splitting approach," *IEEE Transactions on Communications*, vol. 61, no. 9, pp. 3990–4001, Sep. 2013.

[36] X. Zhou, R. Zhang, and C. K. Ho, "Wireless information and power transfer: Architecture design and rate-energy tradeoff," *IEEE Transactions on Communications*, vol. 61, no. 11, pp. 4754–4767, Nov. 2013.

[37] H. Ju and R. Zhang, "Throughput maximization in wireless powered communication networks," *IEEE Transactions on Wireless Communications*, vol. 13, no. 1, pp. 418–428, Jan. 2014.

[38] K. Ishibashi, H. Ochiai, and V. Tarokh, "Energy harvesting cooperative communications," in *IEEE International Symposium on Personal, Indoor and Mobile Radio Communications (PIMRC'12)*, 2012.

[39] C. Huang, R. Zhang, and S. Cui, "Throughput maximization for the gaussian relay channel with energy harvesting constraints," *IEEE Journal on Selected Areas in Communications*, vol. 31, no. 8, pp. 1469–1479, Aug. 2013.

[40] K. Tutuncuoglu, B. Varan, and A. Yener, "Energy harvesting two-way half-duplex relay channel with decode-and-forward relaying: Optimum power policies," in *18th IEEE Int. Conf. Digital Signal Process.*, Jul. 2013.

[41] A. A. Nasir, X. Zhou, S. Durrani, and R. A. Kennedy, "Relaying protocols for wireless energy harvesting and information processing," *IEEE Transactions on Wireless Communications*, vol. 12, no. 7, pp. 3622–3636, Jul. 2013.

[42] A. A. Nasir, X. Zhou, S. Durrani, and R. A. Kennedy, "Wireless-powered relays in cooperative communications: Time-switching relaying protocols and throughput analysis," *IEEE Transactions on Communications*, vol. 63, no. 5, pp. 1607–1622, May 2015.

[43] Z. Ding, S. M. Perlaza, I. Esnaola, and H. V. Poor, "Power allocation strategies in energy harvesting wireless cooperative networks," *IEEE Transactions on Wireless Communications*, vol. 13, no. 2, pp. 846–860, Feb. 2014.

[44] H. Chen, Y. Li, J. L. Rebelatto, B. F. Uchôa-Filho, and B. Vucetic, "Harvest-then-cooperate: Wireless-powered cooperative communications," *IEEE Transactions on Signal Processing*, vol. 63, no. 7, pp. 1700–1711, Apr. 2015.

[45] H. Ju and R. Zhang, "User cooperation in wireless powered communication networks," in *IEEE Global Communications Conference (GLOBECOM)*, Dec. 2014.

[46] A. Host-Madsen and J. Zhang, "Capacity bounds and power allocation for wireless relay channels," *IEEE Transactions on Information Theory*, vol. 51, no. 6, pp. 2020–2040, Jun. 2005.

[47] S. Boyd and L. Vandenberghe, *Convex Optimization*. Cambridge University Press, 2004.

[48] A. Antoniou and W.-S. Lu, *Practical Optimization: Algorithms and Engineering Applications*. Springer, 2007.

[49] D. S. Michalopoulos, H. A. Suraweera, and R. Schober, "Relay selection for simultaneous information transmission and wireless energy transfer: A tradeoff perspective," *IEEE Journal on Selected Areas in Communications*, vol. 33, no. 8, pp. 1578–1594, Aug. 2015.

[50] A. A. Nasir, X. Zhou, S. Durrani, and R. A. Kennedy, "Wireless-powered relays in cooperative communications: Time-switching relaying protocols and throughput analysis," *IEEE Transactions on Communications*, vol. 63, no. 5, pp. 1607–1622, May 2015.